

POLAR CAP ELECTRON DENSITIES FROM  
DE-1 PLASMA WAVE OBSERVATIONS

by

Ann Marie Miller Persoon

A thesis submitted in partial fulfillment  
of the requirements for the degree of  
Master of Science in Physics  
in the Graduate College of  
The University of Iowa

May, 1983

Thesis supervisor: Professor Donald A. Gurnett

Graduate College  
The University of Iowa  
Iowa City, Iowa

CERTIFICATE OF APPROVAL

---

MASTER'S THESIS

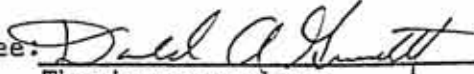
---

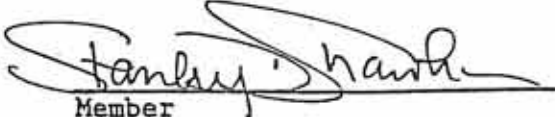
This is to certify that the Master's thesis of


Ann Marie Miller Persoon

has been approved by the Examining Committee  
for the thesis requirement for the Master of  
Science degree in Physics at the May, 1983  
graduation.

Thesis committee:

  
Thesis supervisor

  
Member

  
Member

## ACKNOWLEDGEMENTS

I would like to thank D. B. Muldrew of the Communications Research Centre, Department of Communications, Ottawa, Canada for the use of electron density profiles from the Alouette II and Isis-1 satellites. Density data from these profiles were used to obtain the median profile in Figure 15. I would also like to thank J. E. Jackson of Goddard Space Flight Center and J. Fennel of Aerospace Corporation for their valuable discussions on low-altitude density studies and J. L. Green and J. H. Waite, Jr. of Marshall Space Flight Center for their interesting discussions of ion composition and densities in the polar cap deduced from the Retarding Ion Mass Spectrometer on DE-1.

I would like to express my appreciation to Don Gurnett for his instruction and guidance during my years of study and research. His intuitive insight and helpful suggestions provided the inspiration and direction for this research project and his instructive comments transformed my early awkward efforts into a coherent scientific paper. I would like to thank all of those people whose knowledge and technical skill were largely responsible for transforming my vague ideas and rough sketches into a professional piece of literature: Terry Averkamp whose programming skills converted volumes of data into the instructive plots used in this study; Kathy Goodner whose patience and secretarial skills turned my poor penmanship and numerous rough drafts into

a finished paper; Joyce Chrisinger whose drafting skills changed my imperfect sketches into instructive illustrations; Mark Brown for his fine photography; and Rich Huff and his co-workers for their efforts in obtaining the electric field spectrum measurements used in this study. I would also like to thank all of the faculty members, research scientists, and fellow graduate students who contributed their time, knowledge and patience in countless discussions concerning this research. Their instruction, guidance and support have been invaluable.

This research was supported by NASA through Contracts NAS5-25690 and NAG5-310 with Goddard Space Flight Center, through Grants NGL-16-001-002 and NGL-16-001-043 from NASA Headquarters, and by the Office of Naval Research.

## ABSTRACT

Electric field spectrum measurements from the Plasma Wave Instrument on the Dynamics Explorer-1 spacecraft are used to determine the plasma frequency cutoff of whistler mode radiation at high altitudes over the northern polar cap region. This cutoff provides an accurate (less than 12%) determination of the local electron density. The median electron density over the polar cap at L greater than 10 is found to vary from  $35.2 \pm 8.5 \text{ cm}^{-3}$  at  $2.1 R_E$  to  $0.99 \pm 0.51 \text{ cm}^{-3}$  at  $4.66 R_E$ . Variations up to a factor of four occur from these median values.

The steady state radial outflow model is examined for consistency with the observed density profile. The model predicts an inverse dependence on the product of the plasma velocity and the cube of the radial distance. Comparison of the observed density profile with the radial outflow model yields a power law distribution for the electron density with an exponent of  $-3.85 \pm 0.32$ , which implies a flow velocity increasing nearly linearly with increasing radial distance. Comparison of the observed electron densities with theoretical polar wind densities yields consistent results up to  $2.8 R_E$ , although the steady-state solutions for supersonic  $H^+$  outflow are slightly lower than the observed median densities. Recent DE-1 measurements contradict polar

wind predictions of ion composition and energies, although a thermal polar wind component in the polar cap plasma is also present.

A comparison of observed electron densities with low-altitude density profiles from the Alouette II and Isis-1 spacecrafts indicates a transition in the radial dependence of the electron density at  $1.16 R_E$  and another transition between  $1.55 R_E$  and  $2.0 R_E$ . These transitions are due to changes in the basic processes of plasma transport with increasing radial distance in the polar cap region. A combination of a near diffusive equilibrium distribution and a subsonic outward plasma flow in the high density region below  $1.16 R_E$  becomes a supersonic, collision-dominated outward flux as the plasma density diminishes above  $1.16 R_E$ . A second transition in the density profile is expected between  $1.55 R_E$  and  $2.0 R_E$  when the collision-dominated radial outflow model below  $1.55 R_E$  develops into a collisionless power law distribution in the very low density regions of the polar cap at the height of the DE-1 orbit.

# TABLE OF CONTENTS

	Page
LIST OF FIGURES . . . . .	vii
I. INTRODUCTION . . . . .	1
A. Early Work on Electron Density Measurements . . . . .	2
B. Instrumentation of DE-1 . . . . .	4
II. METHOD OF ANALYSIS . . . . .	6
A. Plasma Wave Modes in the Polar Cap . . . . .	6
B. A Typical Spectrogram: Day 309, 1981 . . . . .	8
C. Identification of Plasma Frequency Cutoff . . . . .	10
D. Measuring the Plasma Frequency Cutoff . . . . .	10
III. REPRESENTATIVE ELECTRIC FIELD SPECTROGRAMS . . . . .	14
A. Day 278, 1981 . . . . .	14
B. Day 047, 1982 . . . . .	15
C. Day 046, 1982 . . . . .	16
D. Day 039, 1982 . . . . .	17
IV. THE ELECTRON DENSITY PROFILE . . . . .	19
V. COMPARISON OF THE DENSITY PROFILES WITH THEORETICAL MODELS . . . . .	22
A. Radial Outflow Model . . . . .	22
B. Polar Wind Solutions . . . . .	26
VI. COMPARISON OF THE HIGH-ALTITUDE DENSITY PROFILE WITH TOPSIDE SOUNDER MEASUREMENTS . . . . .	31
VII. DISCUSSION AND SUMMARY . . . . .	36
REFERENCES . . . . .	40
APPENDIX A: FIGURES . . . . .	43

## LIST OF FIGURES

		Page
Figure 1	A representation of the orientation of the DE-1 orbit in September, 1981, and February, 1982. . . . .	44
Figure 2	CMA diagrams for a two-component plasma for frequencies near the electron gyrofrequency and plasma frequency [Stix, 1962; Chen, 1974]. . . . .	46
Figure 3	A representative spectrogram of electric field amplitude measurements illustrating the various plasma wave emissions found in the polar cap region near the electron gyrofrequency and plasma frequency. . . . .	48
Figure 4	An illustration of representative whistler mode ray paths for sources located in the auroral zone and polar cusp at 1.8 $R_E$ . . . . .	50



		Page
Figure 5	An electric field spectrogram of a polar cusp crossing in early October. . . . .	52
Figure 6	A nightside crossing of auroral field lines in mid-February illustrating a depletion in electron densities at $\lambda_m \approx 50^\circ$ [Calvert, 1981] and a smooth density profile inside the polar cap region. . . . .	54
Figure 7	A continuation of the same polar pass illustrated in Figure 6. . . . .	56
Figure 8	A spectrogram illustrating the time variability of the density profile. . . . .	58
Figure 9	Another nightside crossing of the auroral field lines in early February. . . . .	60
Figure 10	This pass follows the pass illustrated in Figure 9 by eight hours for the region of the polar magnetosphere just poleward of the nightside auroral zone. . . . .	62
Figure 11	A scatter plot of electron density as a function of radial distance. . . . .	64

		Page
Figure 12	A log-log plot of median number densities as a function of radial distance. . . . .	66
Figure 13	Illustration of field-aligned ion flux at high geomagnetic latitudes. . . . .	68
Figure 14	Predicted ion densities below $2.8 R_E$ based on solutions to the 13-moment transport equations [Schunk and Watkins, 1982]. . . . .	70
Figure 15	A log-log plot comparing low-altitude median electron densities obtained from the topside sounder data of Alouette II and Isis-1 and high-altitude median electron densities obtained from the PWI on DE-1. . . . .	72

## I. INTRODUCTION

In this report the electron density profile as a function of radial distance is determined using electric field spectrum measurements from the Plasma Wave Instrument on the Dynamics Explorer-1 spacecraft. The region of interest in this study is the earth's northern polar cap region where geomagnetic field lines are open into the magnetotail and a steady outward plasma flow occurs, resulting in lower electron densities than those observed equatorward of the auroral field lines. The polar cap region is defined to be the region of the magnetosphere poleward of the auroral field lines. Because the auroral zone varies with disturbances in the earth's magnetic field, the northern polar cap region, for purposes of this study, was taken to be that region of the magnetosphere with L-shell values greater than 10, or corresponding invariant latitudes greater than  $71.6^\circ$  ( $\Lambda = \cos^{-1} \sqrt{1/L}$ ).

The Dynamics Explorer-1 spacecraft, launched on August 3, 1981, is in an eccentric polar orbit with perigee and apogee geocentric radial distances of  $1.09 R_E$  and  $4.66 R_E$ , respectively. Because of the eccentricity and range of its orbit and the latitudinal precession of its apogee, this spacecraft provides electric and magnetic field data for a region of the polar magnetosphere not previously studied. Figure 1 illustrates the orientation of the DE-1 orbit in September, 1981, and

the precession of its apogee over the five-month period involved in this study--September, 1981 to February, 1982. The latitudinal precession of the DE-1 apogee is  $108^\circ$  per year. This precession is responsible both for the variations in the altitude of the spacecraft in the polar cap region and for the variations in the length of time the spacecraft spends in this region. During the five-month period covered in this study, the geocentric radial distance of DE-1 in the northern polar cap region varied from  $2.0 R_E$  to  $4.66 R_E$ , or 6378 km to 23,300 km above the earth's surface. This altitude range is far below the high altitude studies of the Hawkeye spacecraft and above the low altitude studies of the Alouette-Isis satellites and the S3-3 spacecraft.

#### A. Early Work on Electron Density Measurements

Prior to 1962, electron density measurements were obtained with the use of ground-based ionosondes [Calvert, 1966]. The bottomside sounding technique employed by the ionosondes was based on the principle of the vertical reflection of pulsed radio waves by ionospheric electron densities, which were related to the sounding frequencies of the waves. The altitude of the reflecting density layers was derived from the measured time delay between the transmitted signal and the reflected echo. This technique was limited to an analysis of electron number densities below the height of maximum ionization of the ionosphere (F2 peak). Transmitted signals with sounding frequencies that exceeded the critical reflection frequency corresponding to this maximum electron density would pass through the ionosphere and would not be reflected. Data from the ground-based ionosondes were used to

construct electron density profiles as a function of altitude only for the region of the ionosphere below the peak of the F2 layer.

To study the electron density profile above the F2 peak, topside sounders, similar in concept and operation to the ground-based ionosondes, were designed to operate on orbiting satellites. The first topside sounder satellite, Alouette I, was launched on September 29, 1962, into a nearly circular polar orbit at 1000 km [Jackson and Warren, 1969; Florida, 1969]. It provided electron density profiles from the F2 peak up to the height of its orbit. This altitude coverage of electron density measurements was expanded to nearly 3000 km by Alouette II, which was launched into an elliptical polar orbit on November 29, 1965 [Jackson and Warren, 1969; Florida, 1969]. Altitude coverage was further expanded by Isis-1 which was launched on January 30, 1969, into an elliptical polar orbit with an apogee of nearly 3500 km [Florida, 1969]. Isis-2, the last satellite in the Alouette-Isis series, was launched on April 1, 1971, into a circular polar orbit at 1400 km. Like its three predecessors, this satellite carried a swept-frequency sounder capable of making the electron density measurements subsequently used to construct vertical electron density profiles. Isis-2 also carried a Langmuir probe instrument, capable of making local measurements of electron density and temperature in the vicinity of the spacecraft [Florida, 1969; Coordinated Ionospheric and Magnetospheric Observations from the Isis 2 Satellite, 1980].

The S3-3 satellite, launched in the summer of 1976, also carried a Langmuir probe instrument to measure electron number densities and density fluctuations along the satellite orbit [Mozier et al., 1979]. The S3-3 orbit was an elliptical polar orbit with an apogee of 8000 km, but electron density measurements in the polar cap region have not yet been published. Above 8000 km, one spacecraft to cross the northern polar cap region was the Hawkeye I spacecraft. It was launched on June 3, 1974, into a highly eccentric orbit with a polar apogee of  $20.5 R_E$ . Due to the precession of its apogee during its four-year lifetime, the Hawkeye spacecraft was able to obtain electric and magnetic field measurements and corresponding charge particle measurements at large radial distances up to  $20 R_E$  in the polar cap region [Gurnett and Frank, 1978]. But, because of the eccentricity of its orbit, there was a gap in the Hawkeye data measurements below approximately  $8 R_E$ . Although density measurements at higher altitudes in the polar cap region could be derived from the Hawkeye electric field measurements [Calvert, 1981], to date no such results have been published.

#### B. Instrumentation of DE-1

The Plasma Wave Instrument (PWI) on Dynamics Explorer-1 has been described in detail in a previous report [see Shawhan et al., 1981]. The instrument is designed to measure AC electric fields over a frequency range of 1 Hz to 2 MHz and an amplitude range of  $0.03 \mu V m^{-1}$  to  $100 mV m^{-1}$ , in addition to magnetic fields and quasi-static electric fields. The antenna system used in measuring these AC electric fields consists of a pair of electric antennas mounted orthogonally to each

other. One 9m tubular antenna is oriented parallel to the spin axis and a 215m long wire antenna is oriented perpendicular to the spin axis. Signals from these sensors are received by two of the PWI receiver systems, the Step Frequency Correlator (SFC) and the Low Frequency Correlator (LFC). The Step Frequency Correlator consists of a correlator and two identical Step Frequency Receivers (SFR) with four frequency bands, each containing 32 frequency steps, scanning a frequency range of 100 Hz to 400 kHz every 32 seconds. The Low Frequency Correlator consists of a correlator and two identical spectrum analyzers with eight filters, scanning a frequency range of 1.78 Hz to 100 Hz every 32 seconds. The resulting electric field amplitude measurements are displayed in frequency-time spectrogram form, covering a two-hour time interval and spanning a frequency range of 1.78 Hz to 400 kHz.

## II. METHOD OF ANALYSIS

### A. Plasma Wave Modes in the Polar Cap

Electric field spectrograms obtained from the electric field amplitude measurements of the PWI illustrate features of the various modes of plasma waves observed by DE-1 for frequencies in the vicinity of the electron gyrofrequency and the electron plasma frequency. There are four plasma wave modes predicted by cold plasma theory for this frequency range [Stix, 1962]. These modes are the free space L-O (left-hand polarized, ordinary) mode, the free-space R-X (right-hand polarized, extraordinary) mode, the Z-mode (extraordinary) and the whistler mode (right-hand polarized). Regions of allowed propagation for these various modes are summarized in the CMA diagrams of Figure 2. These CMA diagrams are derived from the two-component plasma CMA diagrams of Stix [1962, Chap. 2] and Chen [1974, Chap. 4] for a plasma composed of electrons and infinitely massive ions with frequencies near the electron gyrofrequency and the electron plasma frequency. The use of the infinitely massive ion component in this plasma model is justified since the dominant ion for the majority of the polar passes is  $H^+$  and this ion is  $10^3$  times more massive than the electron.

The vertical axis in Figure 2 is the electron gyrofrequency-wave frequency ratio and the horizontal axis is the square of the electron plasma frequency-wave frequency ratio. Figure 2(a) illustrates the



regions of allowed propagation for the free space R-X mode and the Z-mode. The free space R-X mode has a low frequency cutoff at  $f(R=0) = \frac{f_g}{2} + ((\frac{f_g}{2})^2 + f_p^2)^{1/2}$ . The Z-mode is bounded at low frequencies by  $f(L=0) = -\frac{f_g}{2} + ((\frac{f_g}{2})^2 + f_p^2)^{1/2}$  and at high frequencies by the upper hybrid resonance,  $f_{UHR} = (f_g^2 + f_p^2)^{1/2}$ . Figure 2(b) illustrates the regions of allowed propagation for the free space L-O mode and the whistler mode. The free space L-O mode has a low frequency cutoff at the electron plasma frequency. The whistler mode is confined to frequencies below the electron gyrofrequency or the electron plasma frequency, whichever is smaller.

These four plasma wave modes have been associated with electromagnetic plasma wave emissions found in the auroral zone and polar cap region [Gurnett et al., 1983]. Broadband electromagnetic emissions propagating below the electron gyrofrequency in the auroral zone (where  $f_g < f_p$ ) are called auroral hiss. These emissions are believed to be propagating in the whistler mode [Gurnett et al., 1983] because this is the only electromagnetic plasma wave mode propagating in this frequency range (see Figure 2(b)). Auroral hiss is believed to be generated by low energy (100 eV to 10 keV) electrons moving upward along auroral field lines [Gurnett and Frank, 1972] from a region of electron acceleration between  $1.7 R_E$  and  $1.9 R_E$  [Gurnett et al., 1983]. Intense, high-frequency emissions called auroral kilometric radiation (AKR) have also been identified on the PWI electric field spectrograms. This radiation is generated along auroral field lines between  $2 R_E$  and  $4 R_E$  [Gallagher and Gurnett, 1979] and escapes from the earth's

magnetosphere. Recent polarization measurements of AKR by Shawhan and Gurnett [1982] have determined that the dominant component of AKR is right-hand polarized and the radiation propagates in the free space R-X mode. Z-mode radiation has been identified as broadband emissions in the auroral zone by Calvert [1981] and Gurnett et al. [1983]. It can be seen on the following spectrograms that Z-mode radiation extends into the polar cap region with larger bandwidths because of the lower plasma density.

#### B. A Typical Spectrogram: Day 309, 1981

A typical example of an electric field spectrogram illustrating these various wave modes is shown in Figure 3. The trajectory of the spacecraft in a magnetic meridian plane is shown in the lower left corner of the spectrogram. The spacecraft is approaching the nightside auroral region from a radial distance of  $4.2 R_E$  and  $79^\circ$  magnetic latitude and entering the auroral zone at  $47^\circ$  magnetic latitude and a radial distance of  $2.6 R_E$ . Intense emissions in the high frequency range are auroral kilometric radiation, electromagnetic emissions characteristically found in the 100 - 400 kHz frequency range [Shawhan, 1979; Gurnett et al., 1983]. The apparent lower frequency cutoff of auroral kilometric radiation is an instrumentation effect; the low frequency cutoff of the Step Frequency Receivers' fourth frequency band is located at 58 kHz. Emissions in the 15 - 60 kHz range are Z-mode radiation, electromagnetic emissions with a characteristic upper frequency cutoff located at the upper hybrid resonance frequency [Shawhan, 1979; Gurnett et al., 1983]. In this spectrogram, the Z-mode

radiation exhibits a sharply defined upper frequency cutoff at the electron gyrofrequency on the poleward side of the auroral zone. In this region, lower electron densities result in an electron plasma frequency that is much lower than the local electron gyrofrequency. Under these circumstances, the upper hybrid resonance frequency is approximately equal to the local electron gyrofrequency and the latter will become the upper frequency cutoff for the Z-mode.

Intense emissions below 20 kHz which spread out from the auroral region toward the pole are auroral hiss emissions. Auroral hiss is commonly observed between 10 Hz and 100 kHz. Figure 3 illustrates the funnel-shaped lower frequency cutoff of auroral hiss emissions in the auroral zone, a feature that is frequently but not always observed at the altitude of the DE-1 orbit [Gurnett et al., 1983]. Auroral hiss is not confined to the auroral zone but spreads out over a wide range of latitudes on the poleward side of the auroral zone. Stronger damping effects due to the hot magnetospheric plasma in the plasmasphere and plasmopause inhibit the propagation of auroral hiss at lower latitudes. Auroral hiss emissions are also found in the dayside polar cusp (see Figure 5) and exhibit a similar latitudinal asymmetry in the direction of the pole, resulting in a nearly continuous band of emissions over the polar cap region (see Figures 6 and 7). Figure 4 is an illustration of the propagation of auroral hiss emissions into the polar cap region from sources located at approximately  $1.8 R_E$  in the auroral zone and polar cusp. The representative ray paths for a source located at  $1.8 R_E$  have been determined by Gurnett et al. [1983] to fit the lower frequency cutoff of auroral hiss emissions observed by DE-1.

### C. Identification of Plasma Frequency Cutoff

Auroral hiss is whistler mode radiation which, according to plasma wave theory, has a characteristic upper frequency cutoff located at either the electron gyrofrequency or the electron plasma frequency, whichever is smaller [Stix, 1962; Chap. 2; Chen, 1974, Chap. 4]. In the polar cap region, the electron plasma frequency is generally much smaller than the electron gyrofrequency. The electron plasma frequency then gives the upper frequency cutoff for the whistler mode radiation in the polar cap region. In Figure 3, the plasma frequency cutoff is well-defined and varies smoothly from 16 to 19 kHz. It divides the auroral hiss emissions below from the Z-mode radiation above.

### D. Measuring the Plasma Frequency Cutoff

Spectrograms, such as the one in Figure 3, were constructed from the digitized data output of the Step Frequency Receivers. The digitized data was displayed on a video monitor in spectrogram form. A digitizing cursor was used to trace the plasma frequency cutoff on the spectrogram and a frequency value was recorded for each sweep of the Step Frequency Receiver (every 32 seconds). In addition, orbit parameters of the spacecraft, such as magnetic latitude and radial distance, were indexed to each 32-second time interval. From a knowledge of the electron plasma frequency, the electron number density was derived, using the well-known relation:

$$f_p = 9\sqrt{n_e}$$

where  $f_p$  is the electron plasma frequency in kHz and  $n_e$  is the electron number density in  $\text{cm}^{-3}$ .

In addition to using the video monitor and cursor for tracing the plasma frequency cutoff on the spectrogram, the quality of each frequency value was monitored with the use of a quality control index. The index was assigned to each data point in order to isolate data of questionable reliability on spectrograms where the intensity of the whistler mode radiation approached the intensity of the background noise and the upper frequency cutoff was no longer clearly defined. The use of the quality control index made it possible to study the effect of marginally reliable data on the density profile and to locate spurious data points.

For spectrograms in which the upper frequency cutoff was not clearly defined, intensity enhancement techniques were employed to accent the plasma frequency cutoff and minimize background noise and Z-mode radiation. Enhancement techniques were helpful in locating the frequency cutoff when the intensity of the Z-mode radiation approached the intensity of the whistler mode radiation, thereby partially obscuring the plasma frequency cutoff. This effect is evident after 0550 in Figure 3. A 16-point sliding grey scale provided the capability of enhancing the intensity of segments of the frequency range by raising the minimum intensity levels above the maximum intensity of the background noise and lowering the maximum intensity levels displayed on the monitor screen. The remaining narrower intensity range would be spanned by 16 shades from white (lowest intensity) to black (highest intensity). Such enhancement techniques were necessary since the

accurate determination of the electron number density depended on the measurement of a well-defined plasma frequency cutoff.

The combined use of intensity enhancement techniques and tracing the frequency cutoff with a cursor permitted the determination of the frequency cutoff to a high degree of accuracy. The top three SFR frequency bands (900 Hz - 40 kHz) were divided into 96 frequency indices. The cursor could locate the frequency cutoff within a frequency index. At 10 kHz, a typical frequency cutoff value, the frequency cutoff could be determined within  $\pm 600$  Hz, corresponding to an uncertainty in the calculated number density of  $\pm 12\%$ . This uncertainty is negligible compared to the observed spread in density values due to diurnal and latitudinal variations, as well as anticipated large scale variations, due to magnetic field activity and the solar sunspot cycle.

A smaller source of error comes from the identification of the cutoff frequency with the electron plasma frequency. Hot plasma effects such as cyclotron damping and Landau damping can cause the whistler mode wave to cut off at frequencies below the electron plasma frequency. These effects, however, are expected to be small. Because of the small resonance angle of the whistler mode at resonance and the subsequently high index of refraction required for Landau damping, this effect will only be significant in a narrow band of frequencies just below the plasma frequency. Only particles with frequencies in this band will resonate with the wave. For frequencies in the range of  $f_p \pm 2$  kHz, the Landau damping effect would imply an error in the calculated number density of approximately 5% for  $f_p = 10$  kHz. Cyclotron damping will have a significant effect on the cutoff frequency only in the

region of the electron gyrofrequency. A statistical comparison of the electron gyrofrequency and the observed cutoff frequency on the electric field spectrograms indicated that the cutoff frequency was equal to or greater than  $0.9 f_g$  for less than 10% of all data points over most radial distances in this study (see Section IV). Consequently, the cyclotron damping effect implies an error in the calculated number density of less than 3% for 7% of all density data points. The effect is expected to be much smaller than the Landau damping effect.

The method of determining the electron number density from a measured plasma frequency cutoff has a significant inherent limitation. The plasma frequency can be determined with the aforementioned accuracy only for those spectrograms where the cutoff is reasonably well-defined. Of the more than 750 electric field spectrograms examined in this study, only 40% have observable upper frequency cutoffs for at least some fraction of the two-hour time interval of the spectrogram. The quality of the upper frequency cutoff on these spectrograms varies with the intensity of the whistler mode radiation as well as the background noise and the other plasma wave modes propagating near the upper frequency cutoff. The quality of the frequency cutoff was particularly biased toward the lower polar latitudes. Few well-defined frequency cutoffs could be found for magnetic latitudes above  $85^\circ$ . The intensity of auroral hiss emissions propagating into the polar cap from lower auroral latitudes diminishes with increasing latitude. Frequently, at high polar latitudes, auroral hiss emissions could not be distinguished from the background noise.



### III. REPRESENTATIVE ELECTRIC FIELD SPECTROGRAMS

#### A. Day 278, 1981

The electron plasma frequency cutoff, indicated on the spectrogram in Figure 5, is well-defined up until 0840 as the satellite nears the pole. The spectrogram is from early October, 1981, when the satellite's apogee had precessed about  $15^\circ$  to the dayside of the pole. The panel in the lower left-hand corner of the spectrogram indicates the satellite's trajectory. DE-1 is emerging from the dayside polar cusp at  $4.3 R_E$  with a magnetic latitude of  $59^\circ$  and approaching the pole at  $4.6 R_E$  and  $78^\circ$  magnetic latitude at 0858 where there is a data gap. Intense AKR is again evident above 100 kHz and Z-mode radiation, less intense than it was in Figure 3, is found between 10 kHz and 20 kHz at 0755. As in Figure 3, the auroral hiss emissions are latitudinally asymmetric, spreading out over the polar cap region in the direction of the pole. However, the funnel-shaped lower frequency cutoff of the auroral hiss in the auroral zone is not evident in this spectrogram. Below  $78^\circ$  magnetic latitude, the electron plasma frequency is smoothly varying, decreasing with increasing radial distance. Exceptions are the sharp spike in the plasma frequency cutoff at 0752 and several spikes after 0845, indicating a sudden increase in the electron number density by more than a factor of two.



### B. Day 047, 1982

The two spectrograms in Figures 6 and 7 were chosen to illustrate one continuous pass of DE-1 over the polar cap. This pass occurred in mid-February of 1982 when the spacecraft apogee had precessed into the nightside auroral zone. In Figure 6, the spacecraft is in and emerging from the auroral zone as illustrated in the panel in the bottom left-hand corner of the spectrogram. It passes through apogee at approximately 0350 and emerges from the auroral zone shortly after 0400, with a range in magnetic latitude of  $34^{\circ}$  to  $69^{\circ}$ . In the polar cap region, the plasma frequency cutoff of the whistler mode radiation is sharply defined and constant at approximately 10 kHz. The Z-mode radiation above the auroral hiss is less intense and again exhibits a sharp upper-frequency cutoff at the electron gyrofrequency.

The spectrogram in Figure 7 is a continuation of the two-hour spectrogram in Figure 6. The spacecraft is in the northern polar cap region for most of this time interval, passing over the pole at approximately 0600. The vertical white lines on the spectrogram indicate short data gaps. The radial distance of the spacecraft for this spectrogram varies from  $4.4 R_E$  with a magnetic latitude of  $62^{\circ}$  on the nightside of the pole to  $1.8 R_E$  with a magnetic latitude of  $44^{\circ}$  on the dayside of the pole. The spacecraft enters the polar cusp at approximately 0640, as indicated by the onset of broadband auroral hiss emissions at that time. The plasma frequency cutoff in Figure 7 is again sharply defined and is generally constant at about 16 kHz before the spacecraft crosses the pole. However, there is an abrupt 12% decrease in magnitude at a magnetic latitude of  $84^{\circ}$  on the dayside of the pole

(at 0604) and a steady increase in the plasma frequency after 0625 with decreasing radial distance. Generally, though, the plasma frequency in Figures 6 and 7 exhibits few variations on a short time scale and the resulting electron density profile for this orbital pass is smoothly varying.

### C. Day 046, 1982

However, the plasma frequency is not smoothly varying for the orbital pass which immediately precedes the pass illustrated in Figures 6 and 7. In Figure 8 the spacecraft is in the same region of the polar magnetosphere as it is in Figures 6 and 7, only 5 hours earlier. As indicated in the panel in the lower right-hand corner, DE-1 is emerging from the nightside auroral zone into the northern polar cap region. In this two-hour interval, the radial distance of the spacecraft varies from  $4.4 R_E$  with a magnetic latitude of  $47^\circ$  on the nightside of the pole to  $1.8 R_E$  with a magnetic latitude of  $51^\circ$  on the dayside of the pole.

The radiation seen below 50 kHz in Figure 8 is electromagnetic and propagates at frequencies below the electron gyrofrequency in a region of the polar magnetosphere where  $f_p \ll f_g$ . Whistler mode radiation is the only electromagnetic plasma wave mode that can propagate in this frequency range (see Figure 2b)). This whistler mode radiation, however, is not the usual type of auroral hiss associated with the auroral zone since it is believed to be generated at high magnetic latitudes poleward of the auroral field lines [S. D. Shawhan, personal communication]. This radiation may be associated with the polar cap aurora or other aurora-like processes over the polar cap.

Since this radiation is whistler mode radiation, the upper frequency cutoff visible in Figure 8 is the electron plasma frequency. Unlike the plasma frequency cutoff in Figures 6 and 7, the plasma frequency cutoff in Figure 8 is highly variable on time scales of 8 minutes to less than one minute, indicating variations in the electron number density of an order of magnitude or more on spatial scales of 50 - 1400 km.

#### D. Day 039, 1982

The variability in the character of the electron density profile between successive orbital passes of the spacecraft is again illustrated in Figures 9 and 10. The spectrograms in these figures are from successive passes of the spacecraft, emerging from the nightside auroral zone in early February, 1982. In Figure 9, the spacecraft exits the auroral zone at 0400 at a radial distance of  $4.6 R_E$  and a magnetic latitude of approximately  $45^\circ$  and passes through apogee in the polar cap region about 10 minutes later. In this spectrogram, the electron plasma frequency varies smoothly between 9 kHz and 13 kHz with few abrupt changes on a short-time scale, indicating changes in the electron number density by a factor of 2 or less.

On the following orbital pass (Figure 10) the spacecraft again emerges from the nightside auroral zone at 1140 (approximately 7.5 hours later) at a radial distance of  $4.5 R_E$  and a magnetic latitude of  $50^\circ$ . The radial distance of the spacecraft in the polar cap region for this pass varies from  $4.5 R_E$  with a magnetic latitude of  $50^\circ$  to  $3 R_E$  with a magnetic latitude of  $78^\circ$  on the nightside of the pole. Unlike

the preceding pass, the electron plasma frequency cutoff on this spectrogram is not smoothly varying. There is a general tendency for the plasma frequency to increase in magnitude with decreasing radial distance as the spacecraft nears the pole, as it did in Figure 5. But more striking are the large variations in the magnitude of the plasma frequency on time scales of 5 minutes or less, indicating variations in the electron number density up to one order of magnitude on spatial scales of less than 700 km. The electron density profile for this orbital pass is not as smoothly varying as it was in Figure 9.

#### IV. THE ELECTRON DENSITY PROFILE

To obtain the electron density profile in the northern polar cap region, the electron plasma frequency was numerically determined from the analysis of nearly one hundred 2-hour electric field spectrograms, selected from the five-month time interval of September, 1981, to February, 1982. The electron number density was calculated from the plasma frequency using the relation:  $f_p = 9\sqrt{n_e}$ , where  $f_p$  is in kHz and  $n_e$  is in  $\text{cm}^{-3}$ . Figure 11 is a semilog plot of the calculated electron number density as a function of radial distance. This plot illustrates the wide scatter in the observed electron density for a given radial distance. The scatter was not unexpected since the electron densities have been obtained over a wide range of magnetic latitudes for a given radial distance. The electron density data also includes a wide range of magnetic field conditions and large variations are observed from orbit to orbit. On the average, during the five months immediately following the launch of DE-1, magnetic activity was relatively high ( $k_p \approx 3$ ), although magnetic field conditions were subject to change on time scales less than the period of the DE-1 orbit. Nevertheless, despite the resulting spread in density values for a given radial distance, the expected decrease in electron density with increasing radial distance is clearly evident.

The observed upper density cutoff in Figure 11 corresponds to the electron gyrofrequency as a function of radial distance. Electron number densities can be determined from the whistler mode cutoff frequency only when the electron plasma frequency is lower than the electron gyrofrequency. When the electron plasma frequency exceeds the gyrofrequency, the electron density calculated from the cutoff frequency (now the electron gyrofrequency) merely represents a lower limit on the actual electron density. A statistical tabulation of the data points for which the cutoff frequency was greater than 90% of the electron gyrofrequency indicated that the electron gyrofrequency contaminated the calculation of electron densities in only 1% of the cases at  $2.0 R_E$  to 11% of the cases for radial distances greater than  $4.0 R_E$ .

To further explore the relationship between electron density and radial distance and to determine the spread in number density values for a given altitude, the radial range was divided into radial increments of  $0.25 R_E$  and the median value of the electron number density was computed for each radial increment. Median values were used to minimize the effect of number density values greater than the gyrofrequency density values. Since the majority of the data points cluster in a band below the "gyrofrequency cutoff" in Figure 11, the median values are negligibly affected by the relatively few discarded density values located above the gyrofrequency cutoff. Figure 12 is a log-log plot of the median electron number density as a function of radial distance. The error bars indicate quartiles, illustrating the spread in 25% of the data on either side of the median values. These median number densities range from  $35.2 \pm 8.5 \text{ cm}^{-3}$  at  $2.0 R_E$  to  $0.99 \pm 0.51$

$\text{cm}^{-3}$  at  $4.5 R_E$ . Variations up to a factor of 4 occur from these median values. The calculation of the slope of the best line fit through these median values indicates a power law relationship between the electron number density and radial distance with an exponent of  $-3.85 \pm 0.32$ .

## V. COMPARISON OF THE DENSITY PROFILES WITH THEORETICAL MODELS

### A. Radial Outflow Model

In the high density low-latitude region of the Earth's magnetosphere, plasma is contained on closed magnetic field lines and exists in a state of near-diffusive equilibrium [Dessler and Michel, 1966; Dungey, 1961]. However, diffusive equilibrium solutions are derived from a Maxwellian velocity distribution in a collision-dominated regime [Bauer, 1969]. At high geomagnetic latitudes, electron densities can be very low above  $1.24 R_E$  [Hagg, 1967; Timleck and Nelms, 1969]. Field lines are open to interplanetary space in the magnetotail region where the boundary plasma pressure is very low and an outward flow of ionospheric ions results [Banks and Holzer, 1968, 1969b]. This outward flux of predominantly light ions has been called the polar wind [Axford, 1968].

The existence of an upward, field-aligned flux of protons, predicted by the polar wind theory, was confirmed by Explorer XXXI. The ion mass spectrometer on this satellite, launched simultaneously with Alouette II, detected an upward proton flux in the low plasma density region of the polar cap above 1000 km [Hoffman, 1969; Hoffman and Dodson, 1980]. At the higher altitudes of the DE-1 orbit, the Retarding Ion Mass Spectrometer and the Energetic Ion Composition Spectrometer have both detected a similar flux of lighter ions ( $H^+$  and  $He^+$ ) in the polar cap region [Chappell et al., 1982a; Shelley et al., 1982].



However, a significant flux of  $N^+$  ions [Chappell et al., 1982b] has also been detected, and recent measurements have discovered a peak in the flux of the  $O^+$  ion [Shelley et al., 1982] which appears to be associated with periods of increased magnetic activity with  $k_p > 5$  [J. H. Waite, personal communication].

A simplified illustration of the observed ion flux at high geomagnetic latitudes is shown in Figure 13. Since the ion fluxes detected by DE-1 are field-aligned, the ion flux tube follows the magnetic field geometry. An ion flux perpendicular to the magnetic field lines also exists in this region of the polar magnetosphere due to the magnetic convection cycle [Banks and Holzer, 1969b]. The individual ion continuity equation can be written in the form

$$\frac{\partial n_i}{\partial t} + \vec{\nabla} \cdot (n_i \vec{U}_i) = q_i - \ell_i$$

where  $n_i$  is the ion number density,  $\vec{U}_i$  is the ion flow velocity,  $q_i$  is the ion production rate and  $\ell_i$  is the ion loss rate.

Adopting steady state conditions, the first term tends to zero. Although steady state conditions do not exist at all times in the polar magnetosphere, steady state is a justifiable first-order approximation when density data is time-averaged over several months, minimizing variations on a short time scale. For the low neutral particle density regions of the polar magnetosphere at the height of the DE-1 orbit, the ion loss and production terms are assumed to be negligible so that the continuity equation becomes

$$\vec{\nabla}_{\parallel} \cdot (n_i \vec{U}_{i\parallel}) + \vec{\nabla}_{\perp} \cdot (n_i \vec{U}_{i\perp}) = 0$$

where the terms in parentheses refer to the divergence of the ion flux parallel and perpendicular to the magnetic field. The constancy of the magnetic field in the polar cap requires a zero divergence of the perpendicular flow velocity. Although latitudinal variations in the number density suggest a non-zero divergence in the perpendicular flux, it is assumed, in a first order approximation, that this divergence is negligibly small. With these approximations, the continuity equation of a simple radial outflow model requires that

$$n_i u_i A = \text{constant}$$

where  $u_i$  is the ion flow velocity parallel to the magnetic field and  $A$  is the cross-sectional area of the flux tube at a given radial distance (see Figure 13).

The conservation of magnetic flux requires that

$$AB = \text{constant}$$

where  $B$  is the magnetic field intensity. A first order dipole approximation for the magnetic field in the polar cap region is

$$B \propto R^{-3}$$

This approximation is valid over a considerable radial range in the polar magnetosphere and leads to a relationship between the cross-sectional area of a magnetic flux tube and the radial distance:

$$A \propto R^3$$

The continuity equation for the steady state radial outflow of plasma along magnetic field lines, neglecting ion loss and production, predicts that

$$n_i \propto u_i^{-1} R^{-3}$$

where  $A \propto R^3$  has been substituted for the cross-sectional area of the flux tube in the continuity equation. The condition of electrical neutrality in the polar cap region requires that

$$n_e = \sum_i Z_i n_i$$

where  $Z_i$  is the charge state of the individual ion species. Since  $H^+$  is generally the dominant ion in the polar cap, the leading term in the summation is  $n_{H^+}$  where  $n_{H^+}$  is the singly charged hydrogen ion number density. It follows that, to a first order approximation,  $n_e \approx n_{H^+}$  so that

$$n_e \propto u^{-1} R^{-3}$$

where  $u$  is the plasma flow velocity along the magnetic field line. A constant plasma flow velocity would place an upper limit on the exponent of a power law distribution of  $-3$ :

$$n_e \propto R^{-3} \quad \text{for } u = \text{constant} \quad .$$

This power law distribution is the asymptotic limit of the polar wind solution derived by Banks and Holzer [1968].

The development of steady-state solutions for high-latitude plasma transport by Banks and Holzer [1969a,b] and by Schunk and Watkins [1981, 1982] indicated an increase in the flow velocity with increasing radial distance. Thus, an exponent greater than 3 in Figure 12 is consistent with the expected relationships of radial distance with flow velocity and cross-sectional area in the polar cap region. It is reasonable to expect that  $n_e \propto R^{-\gamma}$  where  $\gamma > 3$ , if a valid power law relationship exists between electron number density and radial distance. Our best data fit in Figure 12,  $n_e \propto R^{-3.85}$ , indicates a plasma flow velocity increasing almost linearly with increasing radial distance.

### B. Polar Wind Solutions

The newly discovered dominance of the oxygen ion for some DE-1 polar passes was unexpected [Shelley et al., 1982]. The classic polar wind theory predicted a large flux of lighter ions along open magnetic field lines at high latitudes, due to low plasma pressure in the geomagnetic tail. It was postulated that the loss of light ions from the

topside polar ionosphere would result in a dominance of the  $O^+$  ion to an altitude of 4000 km to 7500 km. Above this altitude a substantial, though rapidly diminishing, upward  $O^+$  flux would exist to support the dominant  $H^+$  flux through charge-exchange reactions.

In their theoretical study of multi-ion plasma transport at high geomagnetic latitudes, Banks and Holzer [1969b] derived a set of solutions to the standard hydrodynamic transport equations for various neutral atmosphere models and a range of isotropic, equal electron and ion temperatures. At an altitude of 7000 km ( $2.18 R_E$ ), their predicted electron densities ranged from approximately  $80 \text{ cm}^{-3}$  to nearly  $1000 \text{ cm}^{-3}$ . These densities exceed our observed densities at  $2.25 R_E$  by a factor of 5 to 50.

Banks and Holzer [1969b] also derived a set of predicted ion densities for different neutral atmosphere temperatures and a range of equal electron and ion temperatures. Predicted  $O^+$  densities were found to vary from  $10 \text{ cm}^{-3}$  to  $200 \text{ cm}^{-3}$  and  $H^+$  densities from  $90 \text{ cm}^{-3}$  to  $120 \text{ cm}^{-3}$  at 7000 km. The altitude of the transition from dominant  $O^+$  at low altitudes to dominant  $H^+$  at higher altitudes was found to vary between 4000 km and 7500 km, depending on the initial concentration of hydrogen in the neutral atmosphere model.

When electron and ion temperatures were allowed to vary individually and anisotropic temperature distributions were included in the analysis of high-latitude plasma transport, the predicted ion density profiles were altered and the transition to a dominance of the  $H^+$  ion was discovered to occur at even lower altitudes. In 1982, Schunk and Watkins [1982] developed a set of steady-state solutions for the

high-latitude plasma flow in the altitude range of 1500 km to 12,000 km. Their solutions were derived from the 13-moment system of transport equations which included continuity, momentum, internal energy, stress tensor and heat flow equations for electrons and oxygen and hydrogen ions. The solutions were determined for a range of lower boundary conditions which included the  $H^+$  drift velocity, electron and  $H^+$  temperature gradients, ion number densities, electron and  $H^+$  temperatures and heat fluxes for the electrons and ions at 1500 km. Isis-2 provided the measurements of the hydrogen ion number density, drift velocity and temperature at the base reference level and S3-3 provided electron temperature measurements and a range of possible electron temperature gradients at the reference level.

Schunk and Watkins [1982] published ion density predictions both for supersonic ( $M > 1$ ) and subsonic ( $M < 1$ )  $H^+$  outflows where the Mach number  $M$  refers to the ratio of ion flow velocity to the thermal velocity. The 13-moment transport equations predict a significant electron temperature anisotropy ( $T_{e\perp} > T_{e\parallel}$ ) for the supersonic  $H^+$  outflow and an isotropic electron temperature distribution at this altitude range for a subsonic flow. Both sets of ion density predictions are presented in Figure 14 for two lower boundary electron temperature gradients ( $\nabla T_e = 0.1^\circ K km^{-1}$ ,  $\nabla T_e = 1^\circ K km^{-1}$ ). As the boundary electron temperature gradient increases, the solutions for the supersonic  $H^+$  outflow show a decrease in the hydrogen ion density and a slight increase in the oxygen ion density. Charge neutrality demands that

$$n_e = \sum_i Z_i n_i$$

and it can be seen that the sum of the two highest ion densities ( $H^+$  and  $O^+$ ) predicted by these steady-state solutions to the plasma transport equations for supersonic  $H^+$  outflow is within  $\pm 25\%$  of the median electron density values observed by DE-1 above  $2.5 R_E$ . Predicted ion densities for subsonic  $H^+$  outflow, on the other hand, are much higher at  $2 R_E$  than our data would suggest and the ion density profile drops off with increasing radial distance much more slowly than the PWI measurements indicate.

Recent measurements by the DE-1 High Altitude Plasma Instrument have established the existence of a low energy, field-aligned supersonic ion flux in the polar cap and a conic component of the ion flux due to the perpendicular heating of the field-aligned component [Gurgiolo and Burch, 1982]. The low energy, field-aligned ions constitute the classical polar wind as described by Axford [1968]. These measurements suggest that the subsonic  $H^+$  outflow solutions illustrated in Figure 14 are not appropriate in the polar magnetosphere at the altitude of the DE-1 orbit.

Below  $2.5 R_E$  the slightly lower theoretical ion densities based on the polar wind model, illustrated in Figure 14 for supersonic  $H^+$  outflows, are not unexpected since they are derived from the steady-state solutions to the plasma transport equations. The existence of steady-state conditions along polar magnetic field lines is related to the convection of plasma across the polar magnetosphere and to the speed of the magnetic convective cycle [Banks and Holzer, 1969b]. Regions of recently disconnected field lines, where the time delay has not been sufficient to achieve a steady state, can be expected to have higher

number densities than regions deep in the polar cap. Thus, number density can be expected to vary with magnetic latitudes across the polar cap. A rapid convective speed, which shortens the time interval between the merging and reconnection of magnetic field lines, may be sufficiently great to prevent the plasma from achieving a steady-state flow in the polar magnetosphere. Under these circumstances, observed number densities across the polar cap will be generally higher than the number densities predicted by the steady-state solutions. Variations in the number density due to changes in the magnetic latitude or disturbances in the magnetic field on small time scales have been minimized in this study by averaging densities over all polar magnetic latitudes for L-shell values greater than 10 at any given radial distance. The resulting density profile is expected to be higher than the predicted steady-state densities.



## VI. COMPARISON OF THE HIGH-ALTITUDE DENSITY PROFILE WITH TOPSIDE SOUNDER MEASUREMENTS

Figure 15 is a log-log plot of the electron number density as a function of radial distance from  $1.05 R_E$  to  $4.7 R_E$ . Electron densities for geocentric distances of  $1.05 R_E$  to  $1.47 R_E$  are median density values calculated from a random sampling of more than 350 high-latitude ( $\lambda > 80^\circ$ ) density profiles derived from the Alouette II and Isis-1 topside sounder data. Error bars indicate the spread in electron density values for this random sampling of Alouette II profiles (1966-1967) and Isis-1 profiles (1969). The large density variations are due to latitudinal variations in temperature and ionic composition [Nelms and Lockwood, 1967] as well as variations in solar activity and magnetic field conditions.

There is an abrupt change in the nature of the Alouette/Isis density profile at approximately 1000 km ( $1.16 R_E$ ). This transition indicates a change in the basic processes of ion transport in the lower ionosphere. Below 1000 km, conditions of near diffusive equilibrium combined with an outward flux of plasma at subsonic transport speeds are expected to exist [Bauer, 1969]. A diffusive equilibrium model, based on the rapid diffusion of plasma above the F2 peak, predicts an electron density distribution of [Angerami and Thomas, 1964]

$$n_e \propto e^{-z/2h_i}$$

for  $z \approx R-1$

and  $h_i = \kappa T_i / m_i g$

where  $n_e$  is the electron number density,  $R$  is the geocentric radial distance,  $\kappa$  is Boltzmann's constant,  $h_i$  is the scale height of the dominant ion species,  $T_i$  is the ion temperature and  $m_i$  is the ion mass. An analysis of the Alouette/Isis density data below 1000 km yields a plasma scale height of 337 km. This value for the plasma scale height compares favorably with the  $O^+$  scale height of 282 km for a representative ion temperature of 4000°K at an altitude of 1000 km.  $O^+$  is the dominant ionospheric ion at all altitudes below 1000 km and is the leading term in the determination of the plasma scale height.

Although a vertical diffusive equilibrium distribution is a good approximation of the Alouette/Isis density profiles below 1000 km, the applicability of the model is limited in the polar cap region by the existence of geomagnetic field lines that are open into regions of low plasma pressure in the magnetotail [Bauer, 1969]. Such boundary conditions result in an outward plasma flow along the field lines at subsonic transport speeds below 1000 km [Banks and Holzer, 1969b]. In their solutions of the hydrodynamic transport equations for  $H^+$  and  $O^+$ , Raitt et al. [1975] determined that energy losses due to convective plasma motion are significant in determining density distributions between 700 km and 1000 km.

Above 1000 km, a weakening of the charge-exchange reactions between molecules and ions and a decrease in ion-ion friction due to rapidly decreasing densities results in an upward plasma flow along magnetic field lines [Banks and Holzer, 1969b]. This outward flow, even for low-energy, field-aligned ions, has been found to be supersonic [Gurgiolo and Burch, 1982]. The transition to supersonic transport speeds is theoretically expected to occur between 1000 km and 1500 km [Raitt et al., 1975]. However, the assumption of a collisionless plasma valid at the altitude of the DE-1 orbit, is not valid below 3000 km due to the substantially higher densities in this region. Ion transport processes, consequently, are found to depend in a complicated way on gradients in the plasma parameters and Coulomb collision frequencies [Schunk and Watkins, 1981; 1982; Raitt et al., 1975].

In the density data gap which occurs between the Alouette/Isis orbits and the DE-1 orbit, another transition must occur in order to fit the observed density profiles at low and high altitudes. The observed change in the density profile between  $1.55 R_E$  and  $2.0 R_E$  is attributed to the transition from a collision-dominated regime below to a collisionless regime above. In addition to changes in the basic plasma transport processes, transitions in the density profile may also be attributed to changes in the ionic composition and ion acceleration processes in the polar magnetosphere.

The topside sounder data used to derive the median density values observed in Figure 15 are biased toward regions of higher densities ( $> 300 \text{ cm}^{-3}$ ) by the standard methods of deriving electron densities from topside ionograms [Nelms and Lockwood, 1967]. Electron density values

for these profiles were calculated indirectly from the extraordinary wave reflection frequency and the gyrofrequency and upper hybrid resonance frequency [Hagg, 1967; Alouette II Ionospheric Data from Communications Research Centre in Ottawa] for ionograms on which all traces were distinctly visible. This indirect method of deriving density values was employed because the ordinary wave reflection trace at the plasma resonance  $f_p$  was not always observed, especially in low density regions at high latitudes and altitudes where the plasma frequency occasionally fell below the low frequency limit of the satellite's topside sounder.

In regions of very low electron densities and subsequently low plasma frequencies where  $f_p \ll f_g$ , the upper hybrid resonance frequency approaches the electron gyrofrequency and the indirect determination of electron density described above could not be used. Interference between the electron gyrofrequency and the upper hybrid resonance results in a difference or modulation frequency that can be determined from the ionograms and used to calculate electron densities below  $100 \text{ cm}^{-3}$  [Hagg, 1967]. The use of a modulation frequency technique to determine low density values resulted in the discovery of very low electron densities ( $< 100 \text{ cm}^{-3}$ ) for all polar latitudes ( $\lambda_m > 60^\circ$ ) at radial distances of  $1.24 R_E$  to  $1.47 R_E$  for selected ionograms on which the extraordinary wave reflection trace was not distinctly visible [Nelms and Lockwood, 1967; Hagg, 1967]. The inclusion of these very low densities on Figure 15 would lower the error bars of the Alouette/Isis density curve by an order of magnitude above  $1.2 R_E$ . This would reduce the discrepancy between the low-altitude density studies and the

observed DE-1 density values, since the whistler mode frequency cutoff method of determining electron densities is valid for low densities (see Figure 12). A more complete analysis of available topside ionograms would be necessary in order to determine an accurate slope of the electron density profile between  $1.24 R_E$  and  $1.47 R_E$ .

## VII. DISCUSSION AND SUMMARY

Electron densities at  $2.0 R_E$  to  $4.66 R_E$  have been derived from the plasma frequency cutoff of the whistler mode radiation in the polar cap using electric field spectrum measurements from the PWI on the DE-1 spacecraft. A log-log plot of the median density values as a function of radial distance indicates a power law distribution of electron densities, varying as  $R^{-3.85 \pm 0.32}$ . This power law distribution is consistent with a steady state, radial outflow model of ionospheric ions and electrons along polar magnetic field lines. It implies a nearly linear increase in plasma flow velocity with increasing radial distance.

A comparison of observed electron densities with theoretical ion and electron densities based on the classic polar wind model for supersonic ion flow velocities yields consistent results at  $2.5 R_E$  to  $2.8 R_E$ . The theoretical polar wind densities below  $2.5 R_E$  are slightly lower than the observed median densities. This result is not unexpected since conditions of steady-state plasma flow are not expected to exist across the polar cap at all latitudes and at all times.

A comparison of observed electron densities with low-altitude density profiles from the Alouette/Isis topside sounder data indicates several evolutions in the radial dependence of electron distributions in the polar cap. A state of near diffusive equilibrium combined with an outward flux of plasma at subsonic transport speeds below 1000 km

changes to a collision-dominated outward flux of plasma with a transition to supersonic velocities above 1000 km. This transition is clearly evident in the low-altitude density profile at approximately  $1.16 R_E$  (see Figure 15). A second transition is also indicated in the density data gap between  $1.55 R_E$  and  $2.0 R_E$  to account for the changing nature of the density profiles at high and low altitudes in the polar cap. This second transition in the density profile is due to a change from a collision-dominated radial outflow distribution model below  $1.5 R_E$  to a collisionless power law distribution above  $2.0 R_E$ . Other factors affecting the change in the radial dependence of the electron number density include changes in the ionic composition of the plasma as well as changes in the plasma flow velocity and plasma temperature.

Large variations seen in low-altitude electron densities in earlier studies persist at the higher altitudes of the DE-1 orbit. The spread in the density data is the result of averaging over all polar magnetic latitudes and nearly 80 polar passes for the five-month time interval of this study. Such a survey would conceal all density irregularities on a short time scale and would even suppress irregularities of large spatial dimensions which are not consistent across the polar cap at a constant radial distance. Such irregularities in the density profile at low altitudes were discovered by the early topside sounder satellites. Alouette I, in a polar orbit at a constant radial distance of  $1.16 R_E$ , provided evidence of latitudinal, diurnal and seasonal variations in the electron density profile at high geomagnetic latitudes [Nelms, 1966; Thomas et al., 1966]. Superimposed on the monotonic decrease in number density with increasing latitude were

prominent peaks and troughs in the density distribution on spatial scales of several hundred km [Thomas et al., 1966]. In addition, many small scale irregularities in space and time contributed to the spread in the density data. Some large scale irregularities persisted over continuous polar passes in narrow bands of invariant latitude [Sato and Colin, 1969; Chan and Colin, 1969]. In general polar cap density distributions were found to be very irregular and to sensitively depend on magnetic activity, seasonal variations and local time.

Similar irregularities in the density profile are expected to persist at DE-1 altitudes. The previously cited example of density profile variability between successive polar passes (see Figures 6 - 10) are evidence of large density fluctuations in time periods of less than 8 hours. Such a large transformation in the density profile for the same region of the polar magnetosphere is probably due to abrupt changes in the magnetic field activity. Sufficient data to examine seasonal variations in the density profile at DE-1 altitudes are not yet available. Statistically significant density data for seasonal comparisons at the same radial distances in the polar magnetosphere cannot be obtained until the DE-1 orbit has precessed around to the northern polar cap region in the spring of 1985. But sufficient density data already exist to investigate latitudinal density variations in the polar cap region and to compare these results with low-altitude studies of latitudinal density variations in order to determine the radial extent of persistent maxima and minima in the electron density distributions. A further comparison of magnetic activity and the density profile as a function of time is planned in order to determine the



magnitude of the effect of magnetic convection on the electron density distribution at high geomagnetic latitudes and high altitudes.

## REFERENCES

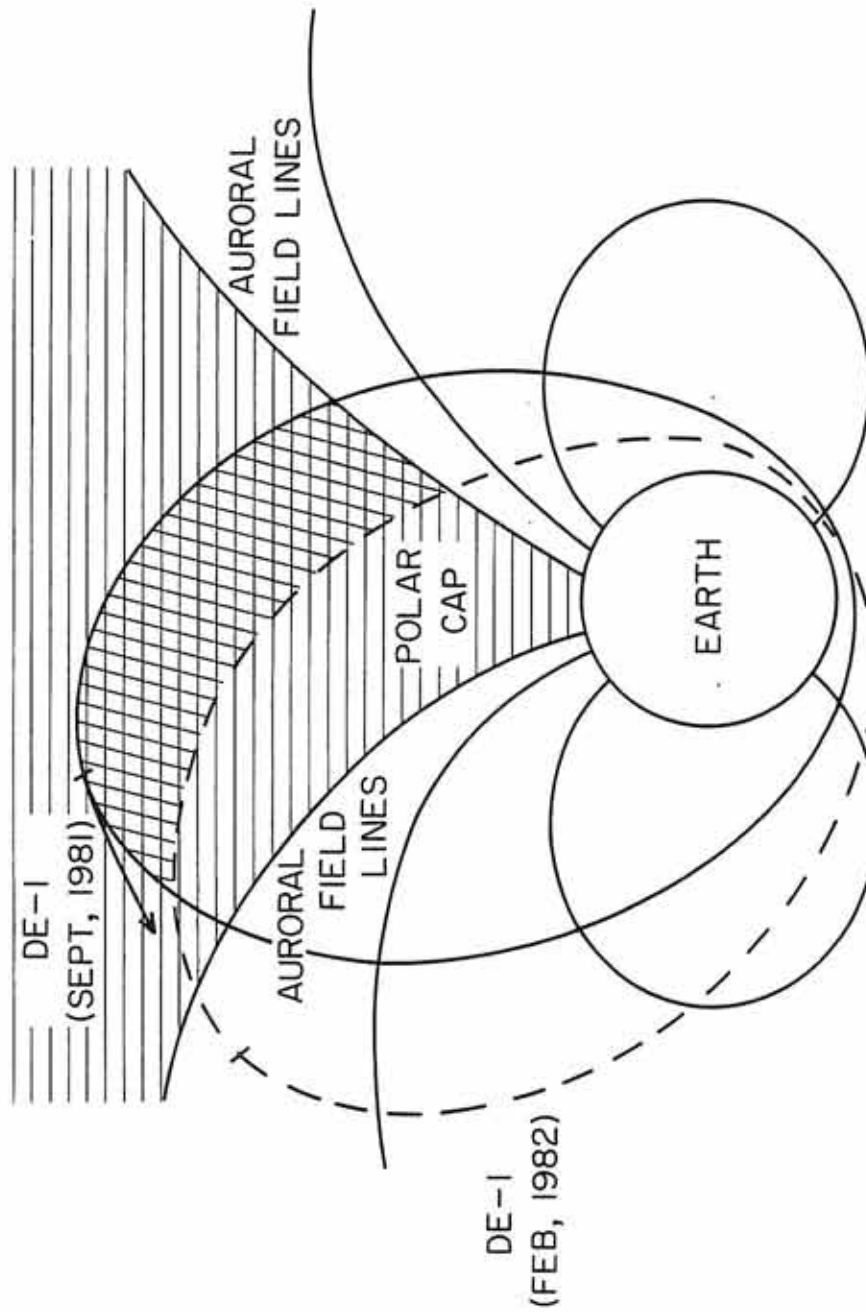
- Angerami, J. J., and J. O. Thomas, The distribution of electrons and ions in the earth's exosphere, J. Geophys. Res., 69, 4537, 1964.
- Axford, W. I., The polar wind and the terrestrial helium budget, J. Geophys. Res., 73, 6855, 1968.
- Banks, P. M., and T. E. Holzer, The polar wind, J. Geophys. Res., 73, 6846, 1968.
- Banks, P. M., and T. E. Holzer, Features of plasma transport in the upper atmosphere, J. Geophys. Res., 74, 6304, 1969a.
- Banks, P. M., and T. E. Holzer, High-latitude plasma transport: The polar wind, J. Geophys. Res., 74, 6317, 1969b.
- Bauer, S. J., Diffusive equilibrium in the topside ionosphere, Proceedings of the IEEE, 57, 1114, 1969.
- Calvert, W., Ionospheric topside sounding, Science, 154, 228, 1966.
- Calvert, W., The auroral plasma cavity, Geophys. Res. Lett., 8, 919, 1981.
- Chan, K. L., and L. Colin, Global electron density distributions from topside soundings, Proceedings of the IEEE, 57, 990, 1969.
- Chappell, C. R., J. L. Green, J. F. E. Johnson, and J. H. Waite, Jr., Pitch angle variations in magnetospheric thermal plasma - Initial observations from Dynamics Explorer-1, Geophys. Res. Lett., 9, 933, 1982a.
- Chappell, C. R., R. C. Olsen, J. L. Green, J. F. E. Johnson, and J. H. Waite, Jr., The discovery of nitrogen ions in the earth's magnetosphere, Geophys. Res. Lett., 9, 937, 1982b.
- Chen, F. F., Introduction to Plasma Physics, Plenum Press Publishing Company, New York, 1974.

- Coordinated Ionospheric and Magnetospheric Observations from the Isis 2 Satellite by the Isis 2 Experimenters, Vol. 3, High-latitude charged particle, magnetic field and ionospheric plasma observations during northern summer, National Space Science Data Center, November 1980.
- Dessler, A. J., and F. C. Michel, Plasma in the geomagnetic tail, J. Geophys. Res., 71, 1421, 1966.
- Dungey, J. W., Interplanetary magnetic field and the auroral zones, Phys. Rev. Lett., 6, 47, 1961.
- Florida C. D., The development of a series of ionospheric satellites, Proceedings of the IEEE, 57, 867, 1969.
- Gallagher, D. L., and D. A. Gurnett, Auroral kilometric radiation: Time-averaged source position, J. Geophys. Res., 84, 6501, 1979.
- Gurgiolo, C., and J. L. Burch, DE-1 observations of the polar wind - A heated and an unheated component, Geophys. Res. Lett., 9, 945, 1982.
- Gurnett, D. A., and L. A. Frank, VLF hiss and related plasma observations in the polar magnetosphere, J. Geophys. Res., 77, 172, 1972.
- Gurnett, D. A., and L. A. Frank, Plasma waves in the polar cusp: Observations from Hawkeye 1, J. Geophys. Res., 83, 1447, 1978.
- Gurnett, D. A., S. D. Shawhan, and R. R. Shaw, Auroral hiss, z-mode radiation and auroral kilometric radiation in the polar magnetosphere: DE-1 observations, J. Geophys. Res., 88, 329, 1983.
- Hagg, E. L., Electron densities of 8-100 electrons  $\text{cm}^{-3}$  deduced from Alouette II high-latitude ionograms, Canadian Journal of Physics, 45, 27, 1967.
- Hoffman, J. H., Ion mass spectrometer on Explorer XXXI satellite, Proceedings of the IEEE, 57, No. 6, 1063, 1969.
- Hoffman, J. H., and W. H. Dodson, Light ion concentrations and fluxes in the polar regions during magnetically quiet times, J. Geophys. Res., 85, 626, 1980.
- Jackson, J. E., and E. S. Warren, Objectives, history, and principal achievements of the topside sounder and Isis programs, Proceedings of the IEEE, 57, 861, 1969.
- Mozer, F. S., C. A. Cattell, M. Temerin, R. B. Torbert, S. Von Glinski, M. Woldorff, and J. Wygant, The dc and ac electric field, plasma density, plasma temperature, and field-aligned current experiments on the S3-3 satellite, J. Geophys. Res., 84, 5875, 1979.

- Nelms, G. L., Seasonal and diurnal variations of the distribution of electron density in the topside of the ionosphere, in Electron Density Profiles in the Ionosphere and Exosphere, ed. by J. Frihagen, North-Holland Publishing Company, Amsterdam, 358, 1966.
- Nelms, G. L., and G. E. K. Lockwood, Early results from the topside sounder in the Alouette II satellite, in Space Research VII, ed. by R. L. Smith Rose, North-Holland Publishing Company, Amsterdam, 604, 1967.
- Raitt, W. J., R. W. Schunk, and P. M. Banks, A comparison of the temperature and density structure in high and low speed thermal proton flows, Planet. Space Sci., 23, 1103, 1975.
- Sato, T., and L. Colin, Morphology of electron concentration enhancement at a height of 1000 km at polar latitudes, J. Geophys. Res., 74, 2193, 1969.
- Schunk, R. W., and D. S. Watkins, Electron temperature anisotropy in the polar wind, J. Geophys. Res., 86, 91, 1981.
- Schunk, R. W., and D. W. Watkins, Proton temperature anisotropy in the polar wind, J. Geophys. Res., 87, 171, 1982.
- Shawhan, S. D., Magnetospheric plasma waves, in Solar System Plasma Physics, Vol. III, ed. by L. J. Lanzerotti, C. F. Kennel and E. H. Parker, North-Holland Publishing Company, 211, 1979.
- Shawhan, S. D., D. A. Gurnett, D. L. Odem, R. A. Helliwell, and C. G. Park, The plasma wave and quasi-static electric field instrument (PWI) for Dynamics Explorer-A, Space Science Instrumentation, 5, 535, 1981.
- Shawhan, S. D., and D. A. Gurnett, The polarization of auroral kilometric radiation by Dynamics Explorer-1, Geophys. Res. Lett., 9, 913, 1982.
- Shelley, E. G., W. K. Peterson, A. G. Ghielmetti, and J. Geiss, The polar ionosphere as a source of energetic magnetospheric plasma, Geophys. Res. Lett., 9, 941, 1982.
- Stix, T. H., The Theory of Plasma Waves, McGraw-Hill Book Company, Inc., New York, 1962.
- Thomas, J. O., M. J. Rycroft, L. Colin, and K. L. Chan, Experimental results from the Alouette I satellite, in Electron Density Profiles in the Ionosphere and Exosphere, ed. by J. Frihagen, North-Holland Publishing Company, Amsterdam, 322, 1966.
- Timleck, P. L., and G. L. Nelms, Electron densities less than 100 electrons  $\text{cm}^{-3}$  in the topside ionosphere, Proceedings of the IEEE, 57, 1164, 1969.

Figure 1      A representation of the orientation of the DE-1 orbit in September, 1981, and February, 1982. All density data presented in this study for this five-month interval are from high-latitude passes over the polar cap region.

A-G83-68-1

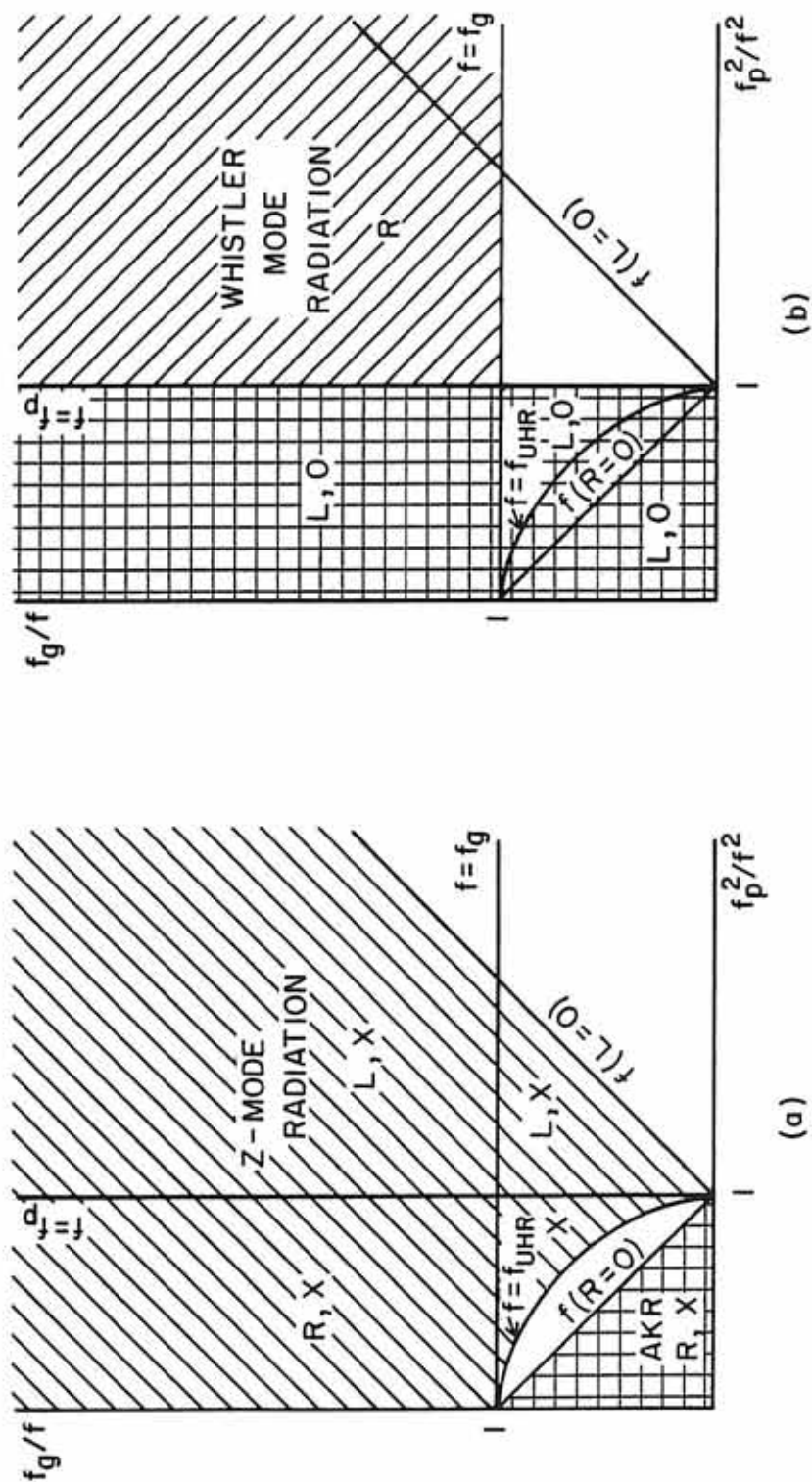


APOGEE ADVANCES IN DE-1 ORBIT OVER A  
5-MONTH INTERVAL

Figure 1

Figure 2 CMA diagrams for a two-component plasma for frequencies near the electron gyrofrequency and plasma frequency [Stix, 1962; Chen, 1974].

Figure 2(a) illustrates the regions of allowed propagation for the free space R-X mode and the Z-mode. Figure 2(b) illustrates the regions of allowed propagation for the free space L-O mode and the whistler mode.



CMA DIAGRAMS FOR A SINGLE ION-ELECTRON PLASMA

Figure 2



Figure 3      A representative spectrogram of electric field amplitude measurements illustrating the various plasma wave emissions found in the polar cap region near the electron gyrofrequency and plasma frequency.

ELECTRIC FIELD, DE-1, NOVEMBER 5, DAY 309, 1981

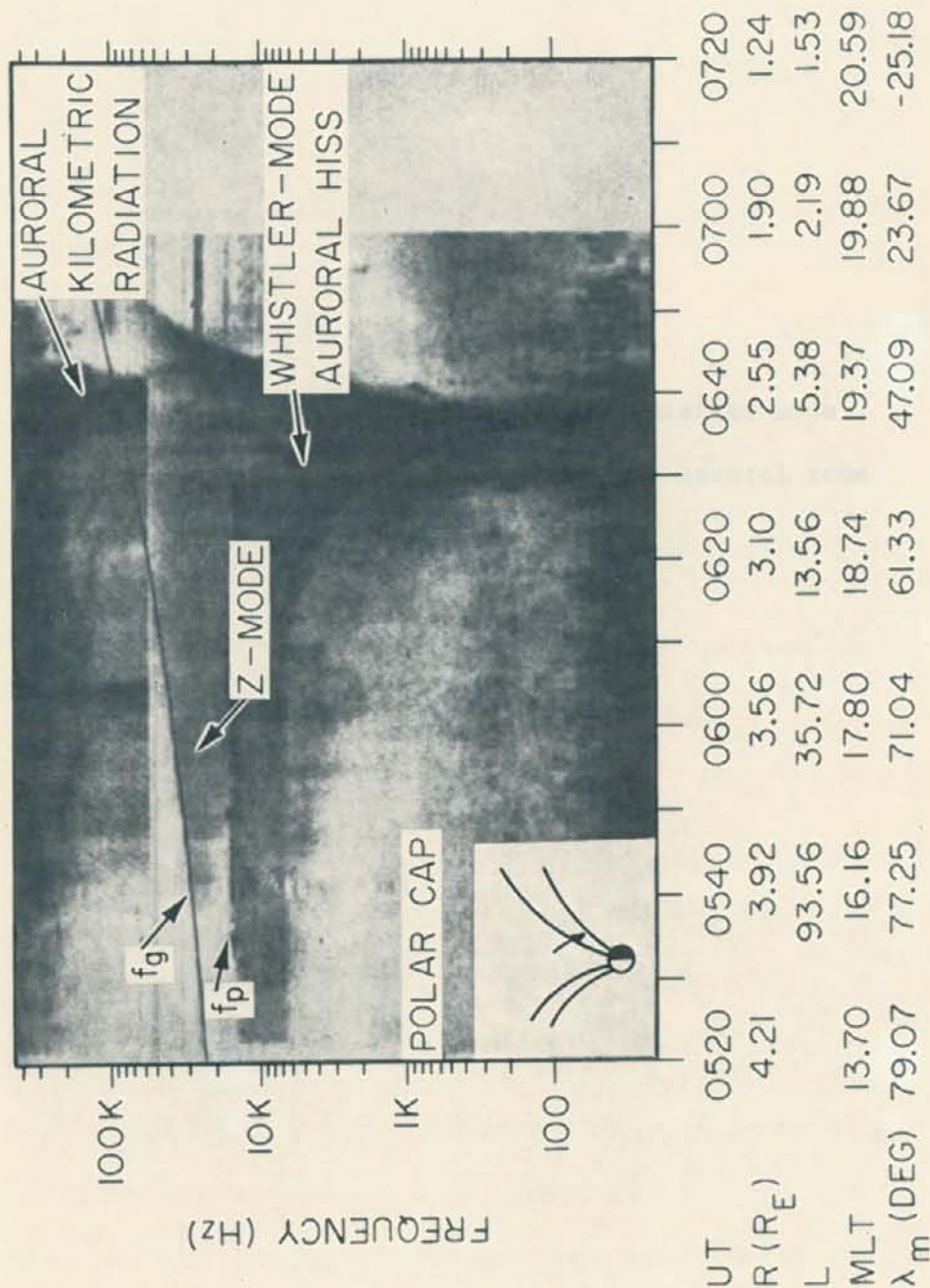


Figure 3

Figure 4      An illustration of representative whistler mode  
ray paths for sources located in the auroral zone  
and polar cusp at  $1.8 R_E$ .

A-G83-379

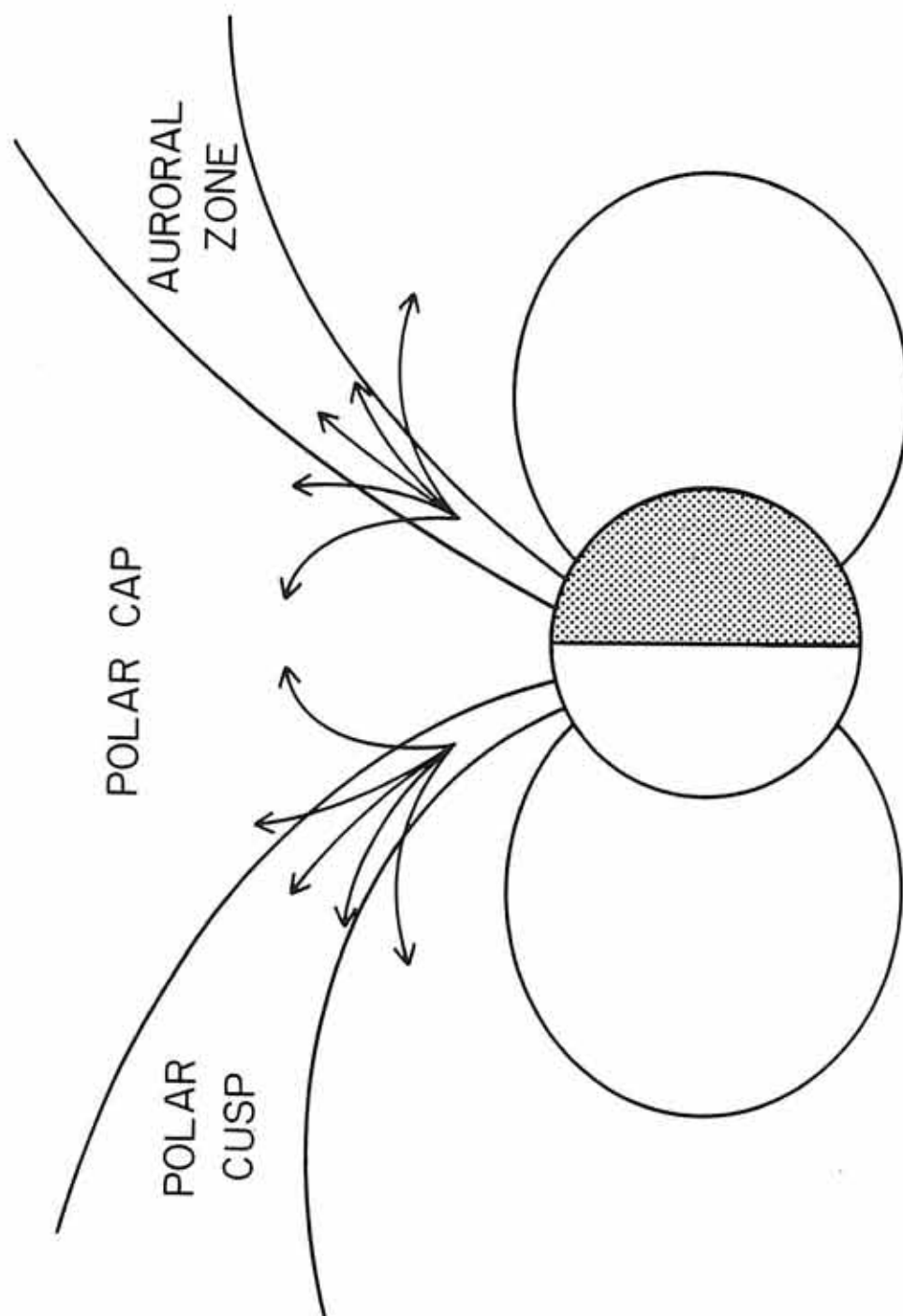


Figure 4

Figure 5

An electric field spectrogram of a polar cusp crossing in early October. Irregularities in the density profile are indicated by sudden increases in  $f_p$  at 0752 and at 0845-0850 as the satellite nears the pole.

ELECTRIC FIELD, DE-1, OCTOBER 5, DAY 278, 1981

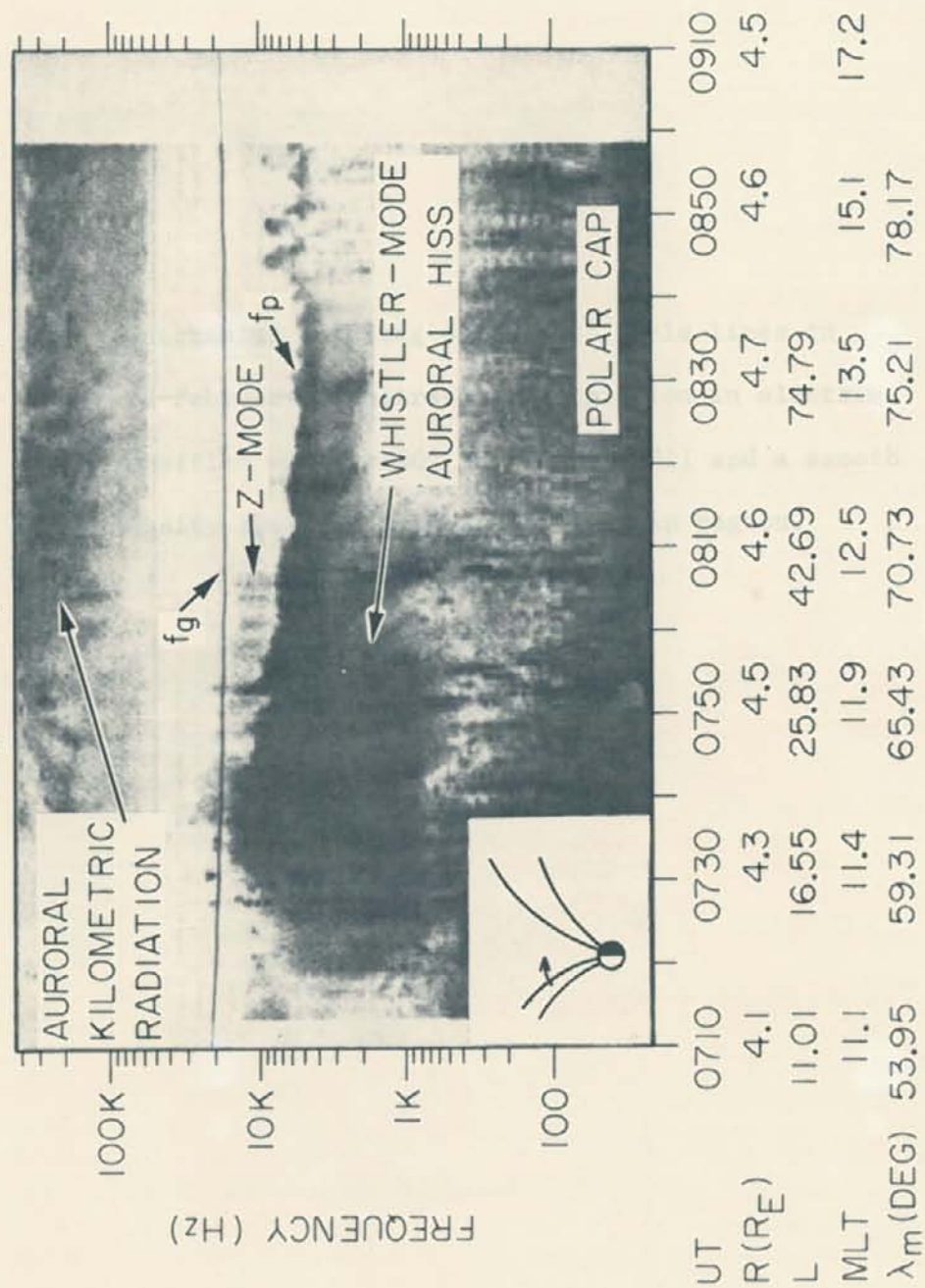


Figure 5

Figure 6      A nightside crossing of auroral field lines in mid-February illustrating a depletion in electron densities at  $\lambda_m \approx 50^\circ$  [Calvert, 1981] and a smooth density profile inside the polar cap region.



A-G82-907-1

ELECTRIC FIELD, DE-1, FEBRUARY 16, DAY 047, 1982

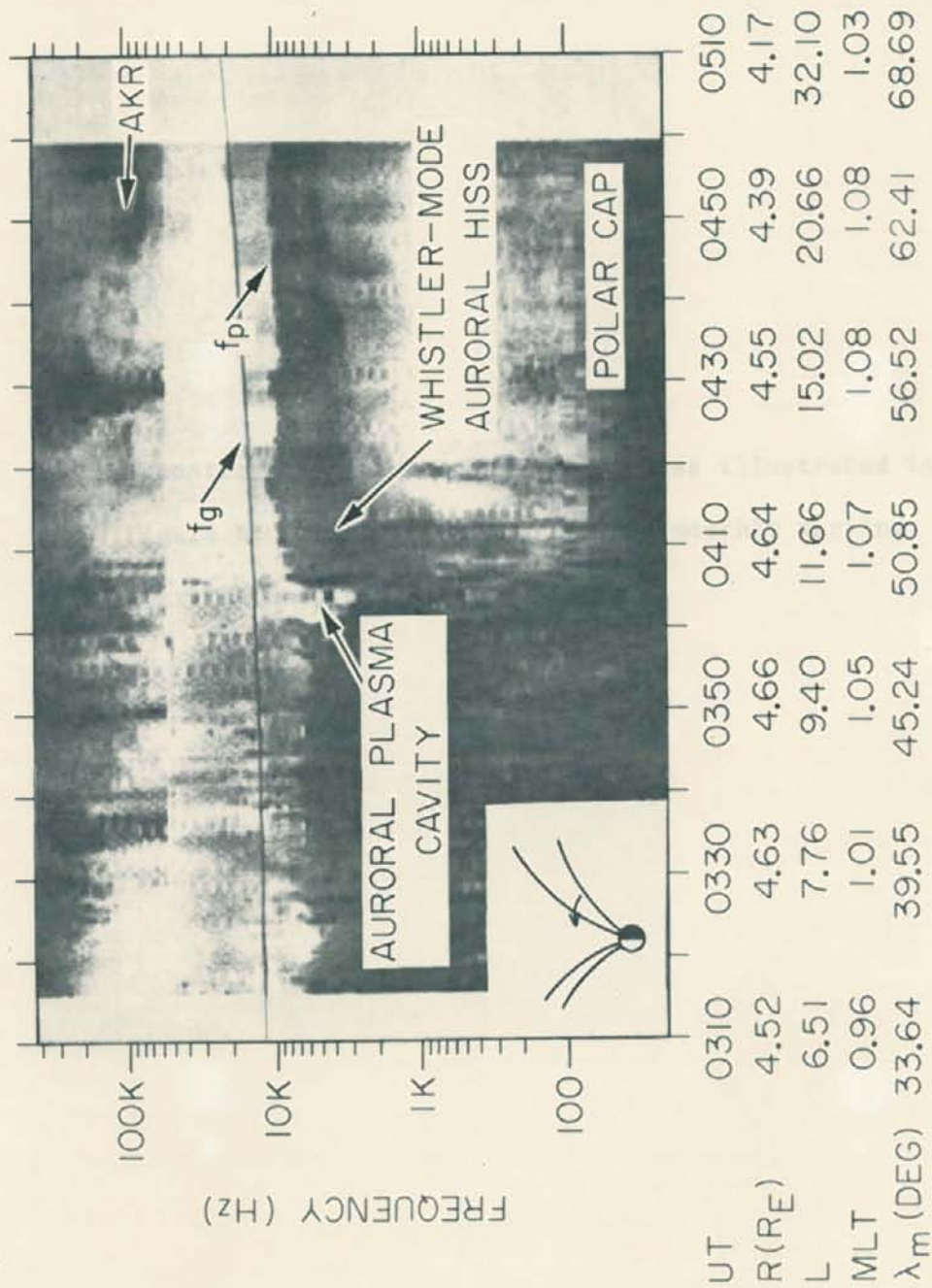


Figure 6



Figure 7                      A continuation of the same polar pass illustrated in Figure 6. The density profile is smoothly varying over the entire polar cap region.

A-G83-214-1

ELECTRIC FIELD, DE-1, FEBRUARY 16, DAY 047, 1982

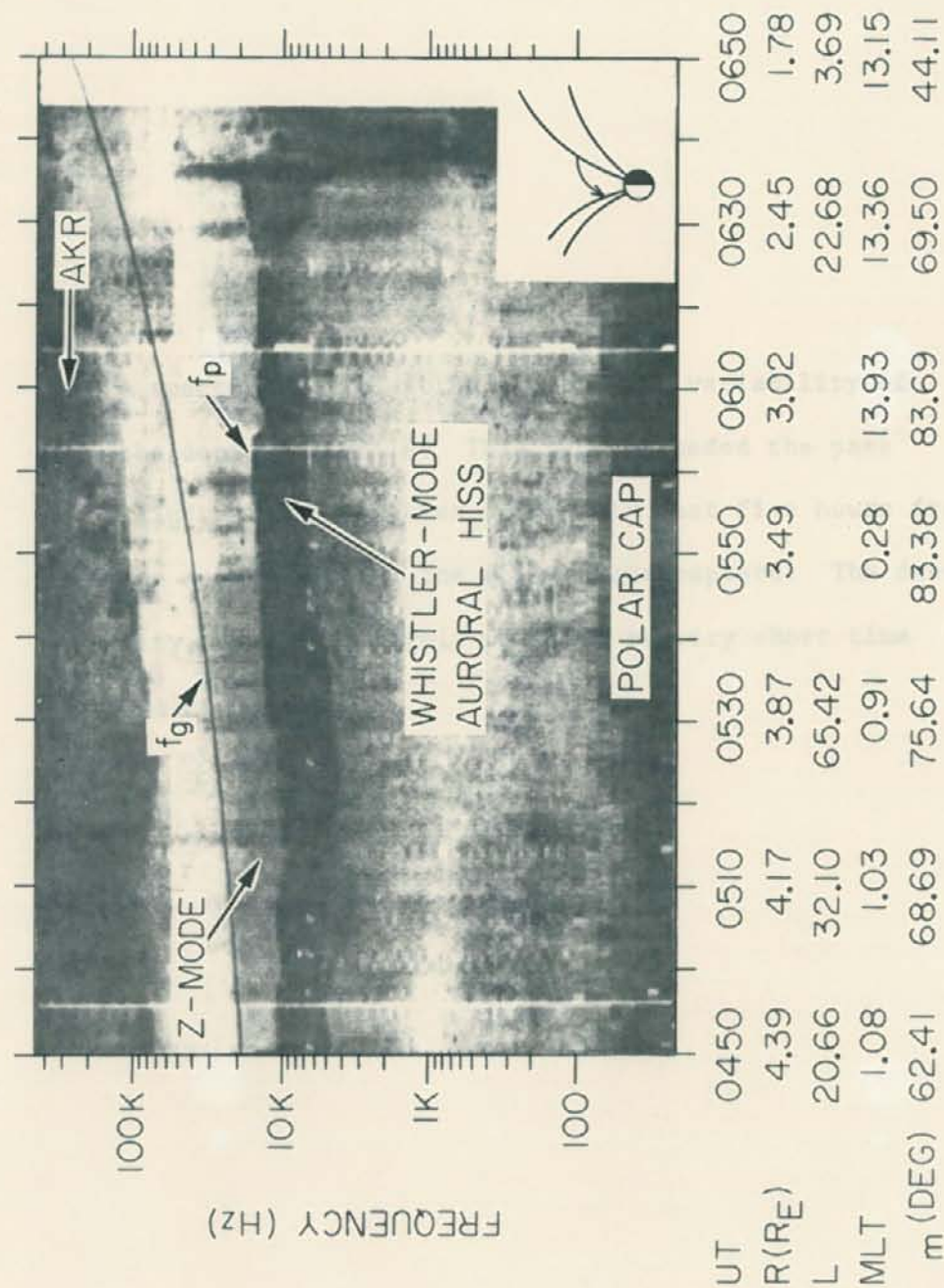


Figure 7

Figure 8

A spectrogram illustrating the time variability of the density profile. This pass preceded the pass illustrated in Figures 6 and 7 by just five hours for the same region of the polar magnetosphere. The density profile is highly variable on very short time scales.

ELECTRIC FIELD, DE-1, FEBRUARY 15, DAY 046, 1982

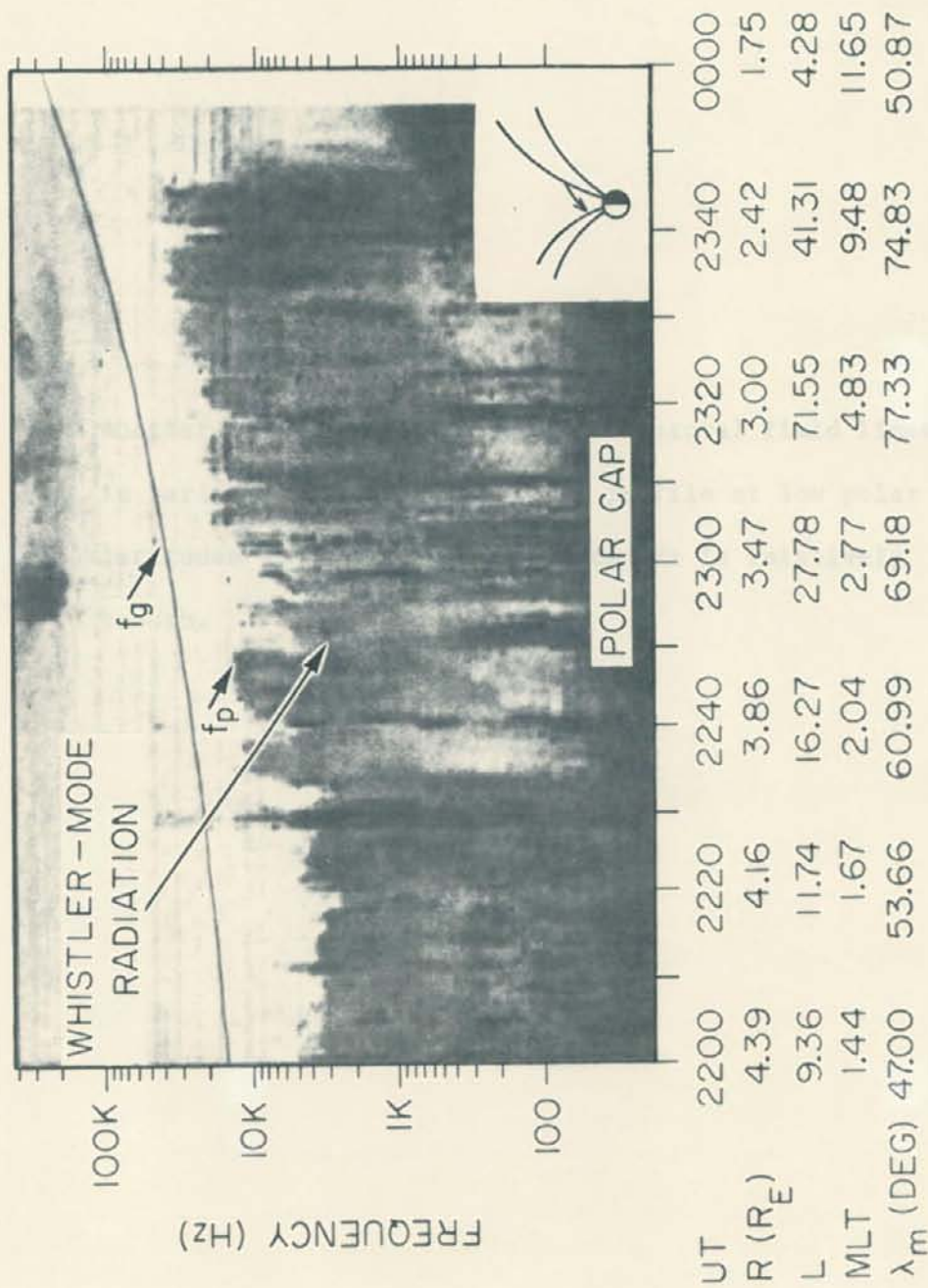


Figure 8

Figure 9

Another nightside crossing of the auroral field lines in early February. The density profile at low polar latitudes above  $50^\circ$  magnetic latitude is relatively smooth.



A-G82-906-1

ELECTRIC FIELD, DE-1, FEBRUARY 8, DAY 039, 1982

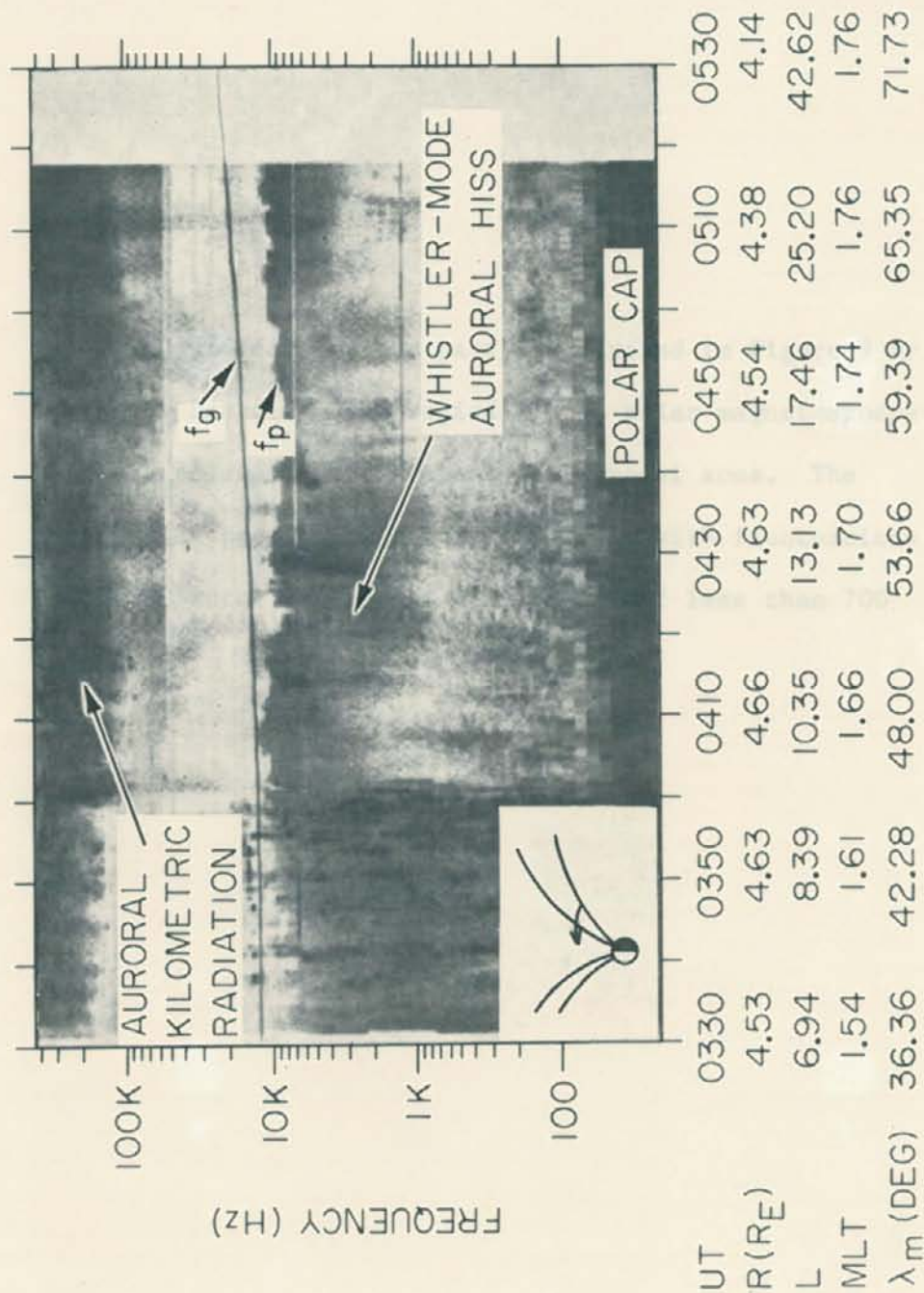


Figure 9

Figure 10

This pass follows the pass illustrated in Figure 9 by eight hours for the region of the polar magnetosphere just poleward of the nightside auroral zone. The density profile is highly irregular with fluctuations by a factor of 2 on spatial scales of less than 700 km.

A-682-911-2

ELECTRIC FIELD, DE-1, FEBRUARY 8, DAY 039, 1982

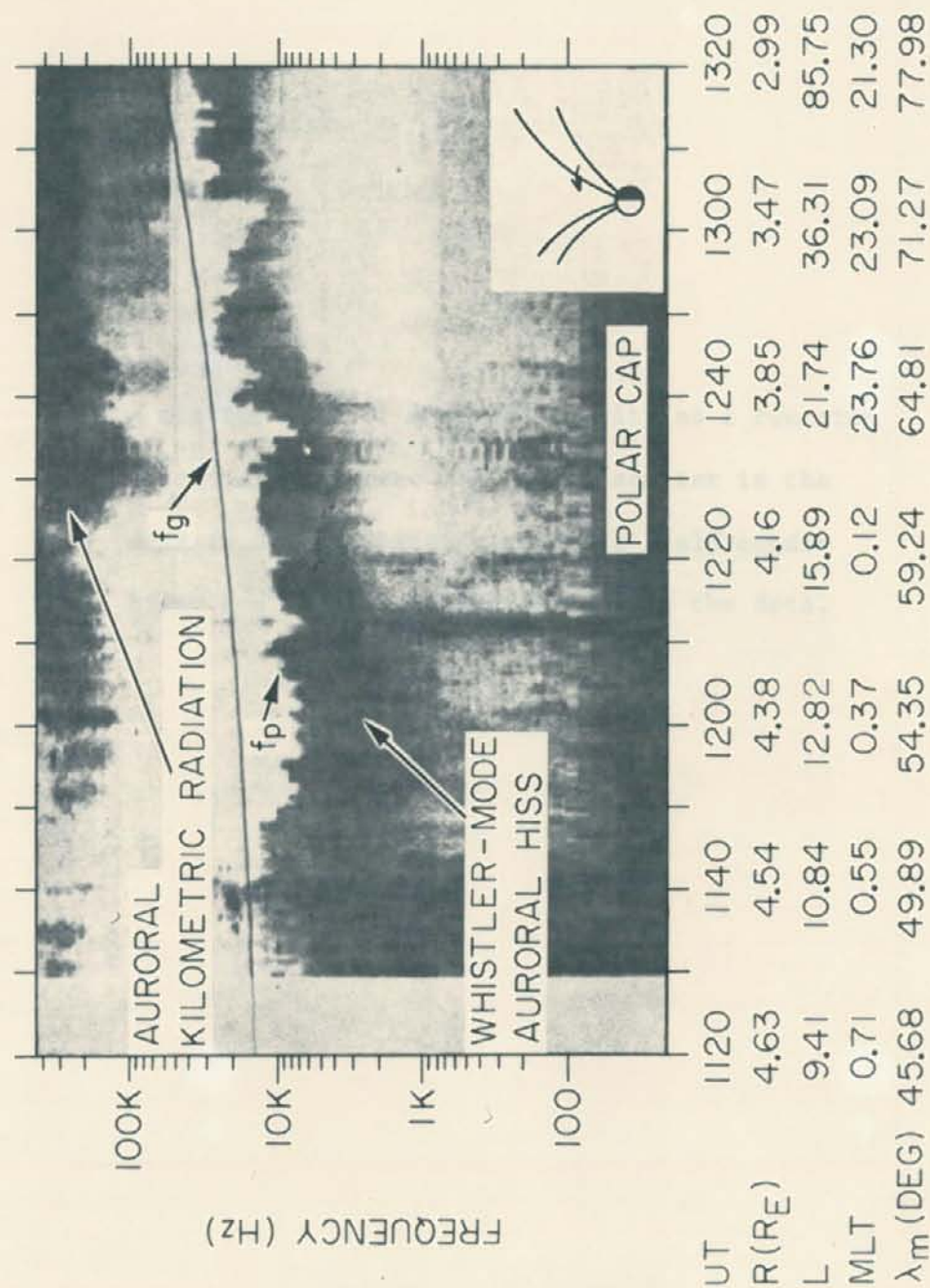


Figure 10



Figure 11      A scatter plot of electron density as a function of radial distance. The large scatter in the data is due to changing magnetic field conditions and latitudinal variations in the data.

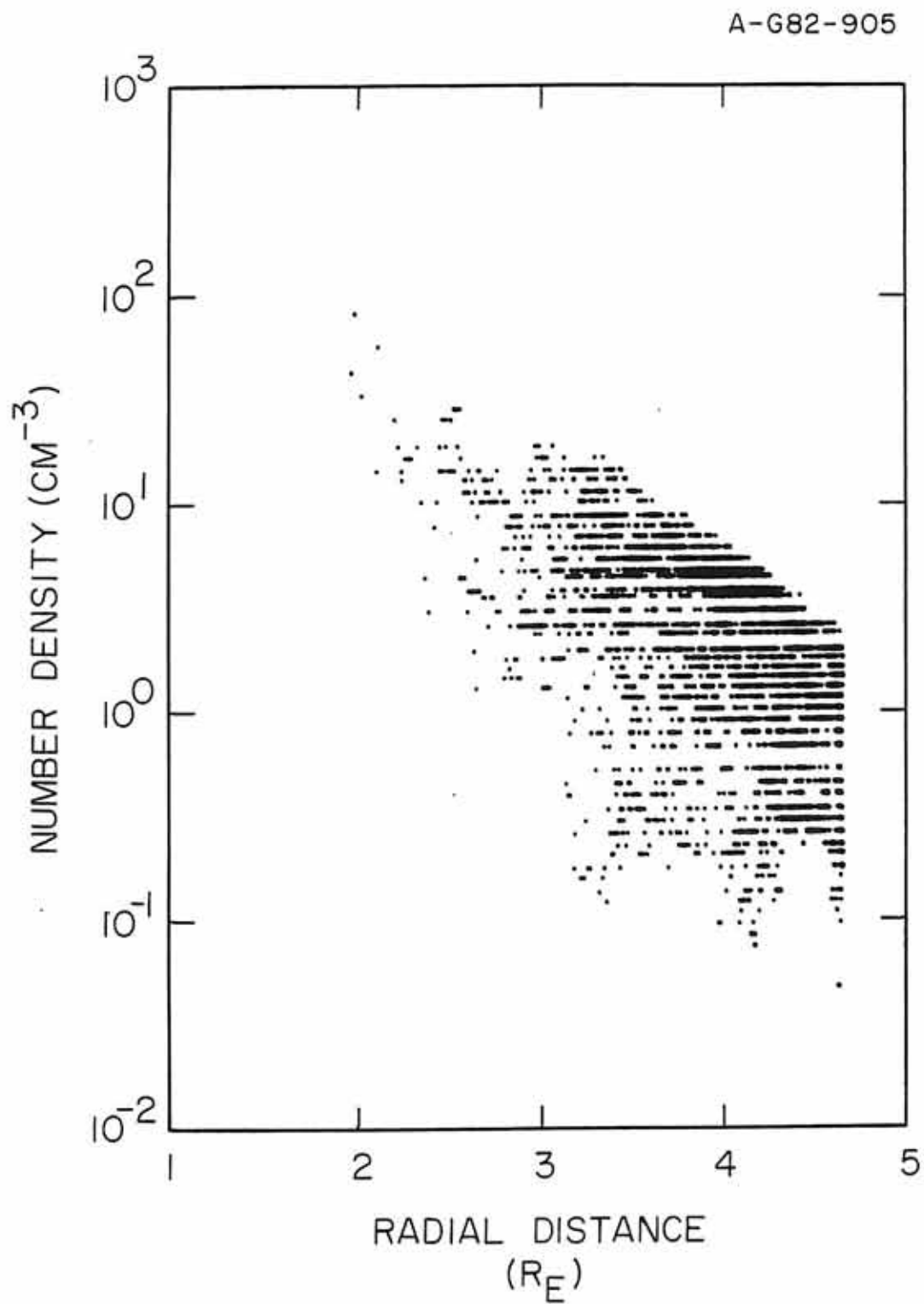


Figure 11

Figure 12      A log-log plot of median number densities as a function of radial distance. The best line fit through these points indicates a power law distribution for electron densities in the polar cap:  $n_e \propto R^{-3.85}$ .

A-G82-904-1

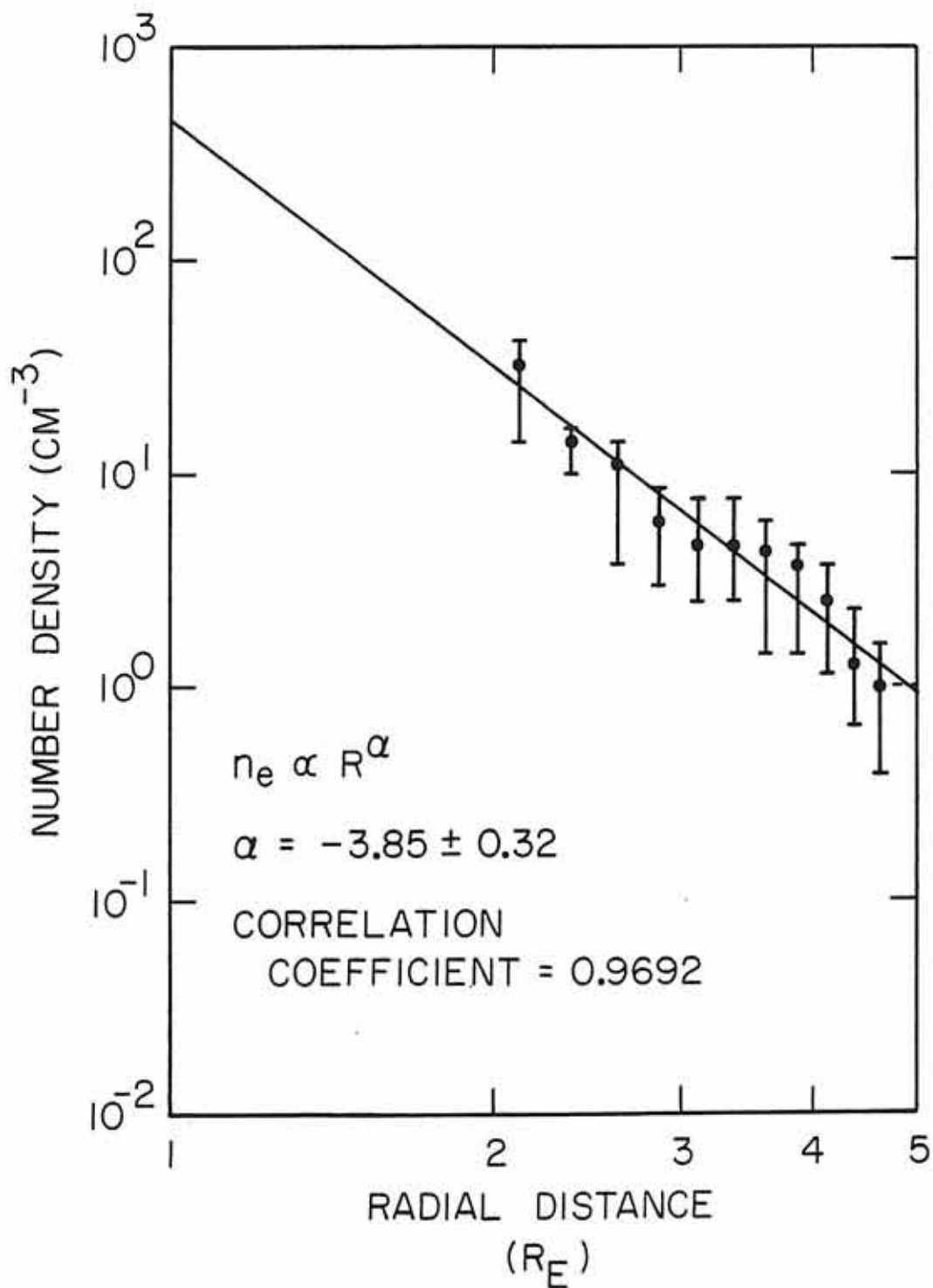


Figure 12

Figure 13

Illustration of field-aligned ion flux at high geomagnetic latitudes.

A-G83-227

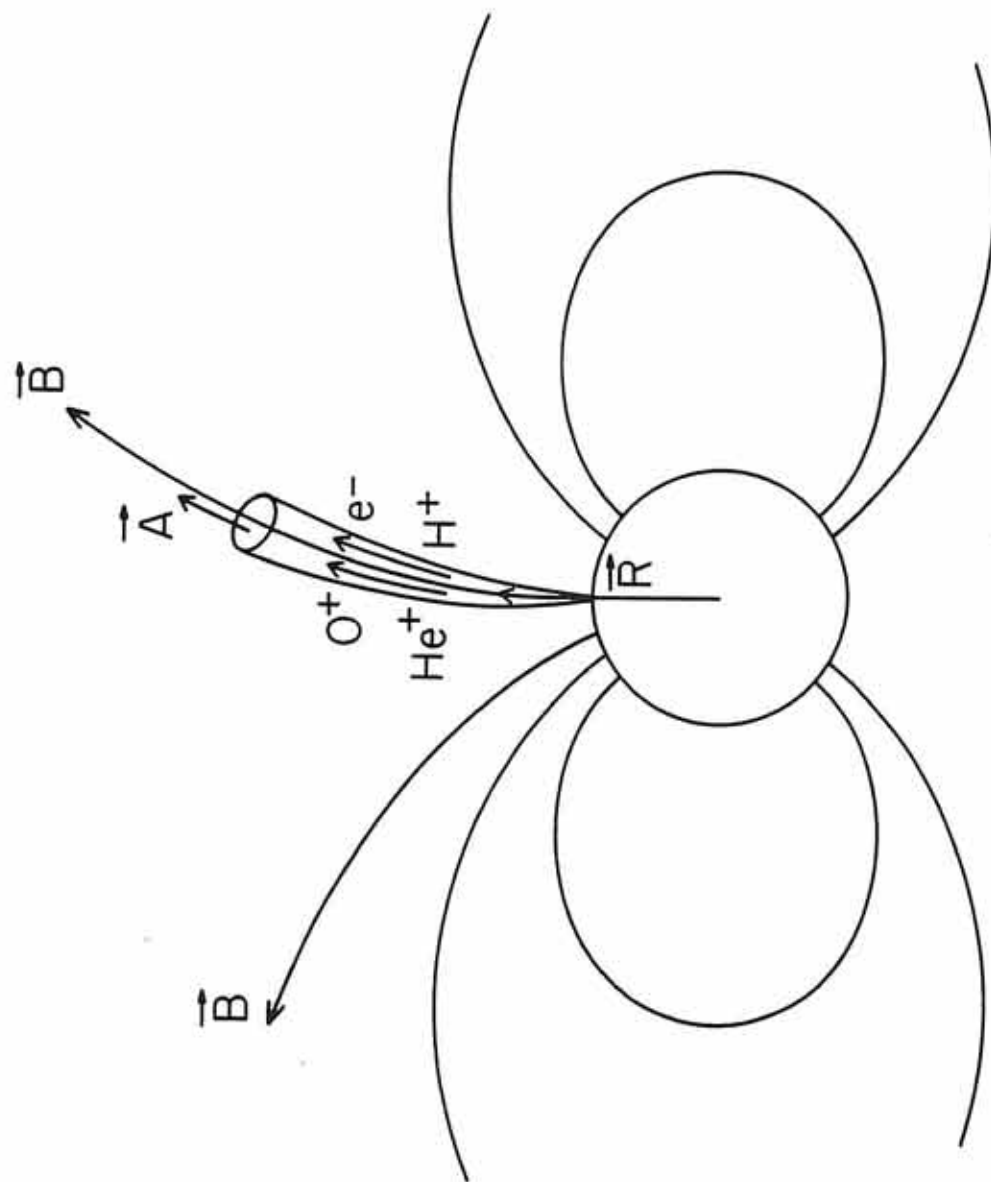


Figure 13

Figure 14

Predicted ion densities below  $2.8 R_E$  based on solutions to the 13-moment transport equations [Schunk and Watkins, 1982]. The subsonic outflow solutions correspond to higher  $H^+$  and  $O^+$  densities. These predicted densities exceed the DE-1 measured densities at  $2 R_E$  by more than an order of magnitude. Supersonic outflow solutions correspond to lower  $H^+$  and  $O^+$  densities. An increase in the boundary electron temperature gradient (from  $0.1^\circ K km^{-1}$  to  $1^\circ K km^{-1}$ ) corresponds to a slight increase in the predicted  $O^+$  densities and a larger decrease in the predicted  $H^+$  densities. Both sets of predicted ion densities for the supersonic outflow solutions are within 25% of the median density values observed by DE-1.

A-G83-228-1

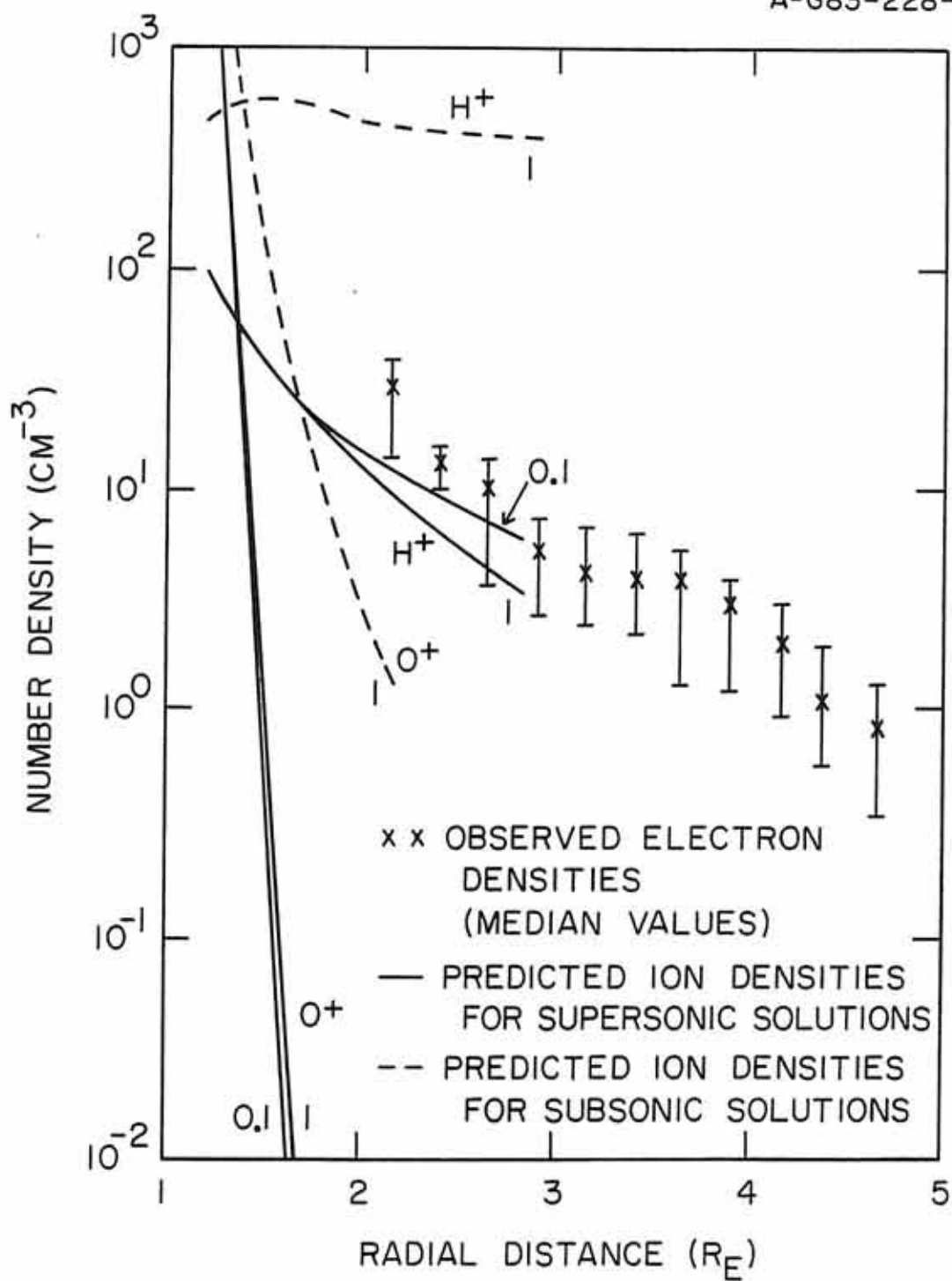


Figure 14



Figure 15      A log-log plot comparing low-altitude median electron densities obtained from the topside sounder data of Alouette II and Isis-1 and high-altitude median electron densities obtained from the PWI on DE-1.

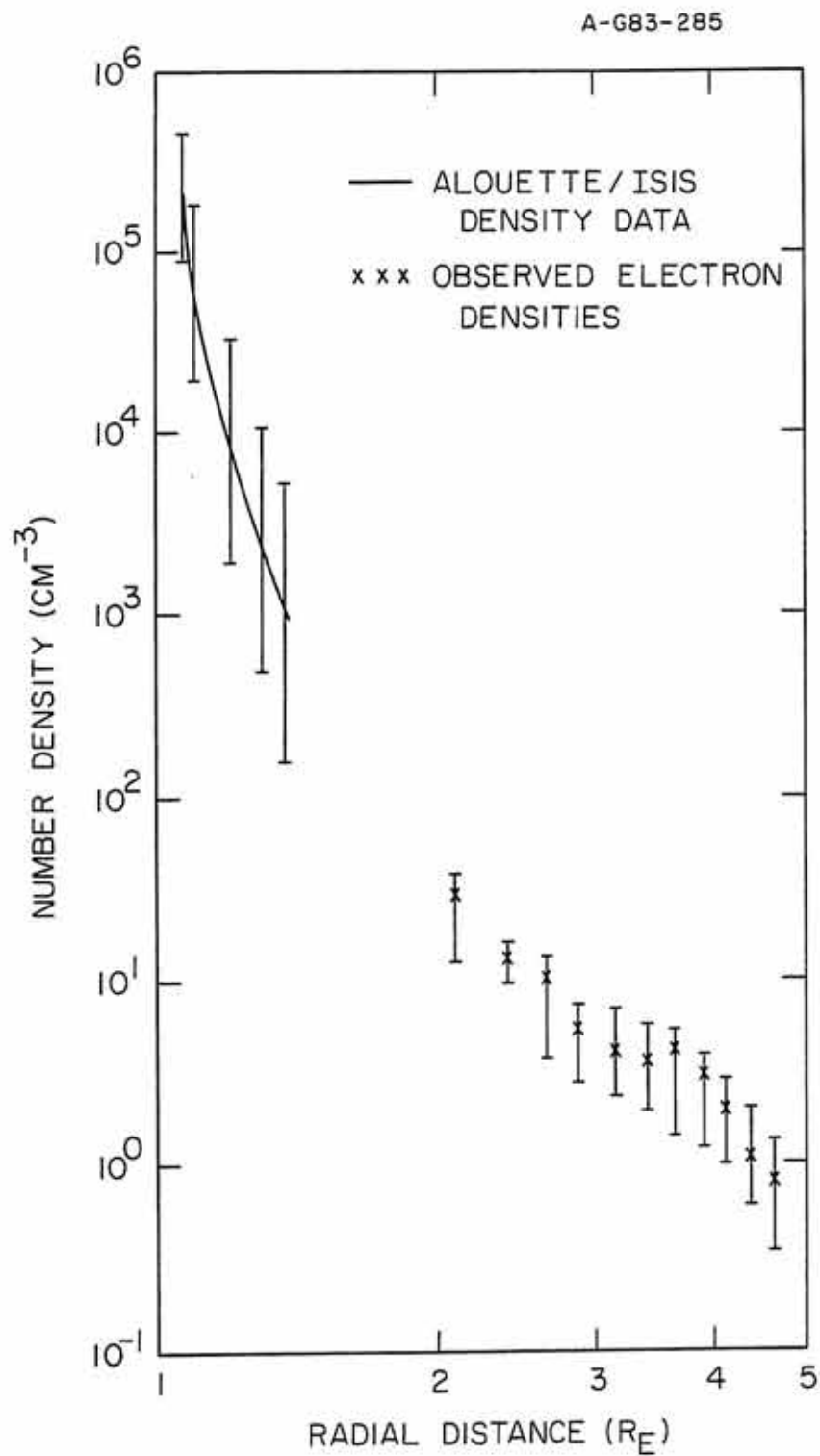


Figure 15